Water Resources Research

RESEARCH ARTICLE
10.1029/2021WR030431

Simulations of Water and Thermal Dynamics for Soil Surfaces With Residue Mulch and Surface Runoff

Zhuangji Wang[1,2], Resham Thapa[2,3], Dennis Timlin[1], Sanai Li[1], Wenguang Sun[1,4], Sahila Beegum[1,4], David Fleisher[1], Steven Mirsky[3], Miguel Cabrera[5], Thomas Sauer[6], Vangimalla R. Reddy[1], Robert Horton[7], and Katherine Tully[2]

[1]Adaptive Cropping System Laboratory, USDA-ARS, Beltsville, MD, USA, [2]Department of Plant Science and Landscape Architecture, University of Maryland, College Park, MD, USA, [3]Sustainable Agricultural Systems Laboratory, USDA-ARS, Beltsville, MD, USA, [4]Nebraska Water Center, University of Nebraska, Lincoln, NE, USA, [5]Department of Crop and Soil Sciences, University of Georgia, Athens, GA, USA, [6]National Laboratory for Agriculture and the Environment, USDA-ARS, Ames, IA, USA, [7]Department of Agronomy, Iowa State University, Ames, IA, USA

Key Points:

- A numerical model is developed to simulate soil surface water and temperature with residue mulch and runoff
- Water and thermal simulations are adaptive to mulch decomposition and shrinkage
- Mulch residue decomposition and N mineralization rate are estimated by the model

Correspondence to:
D. Timlin,
dennis.timlin@usda.gov

Citation:
Wang, Z., Thapa, R., Timlin, D., Li, S., Sun, W., Beegum, S., et al. (2021). Simulations of water and thermal dynamics for soil surfaces with residue mulch and surface runoff. *Water Resources Research*, *57*, e2021WR030431. https://doi.org/10.1029/2021WR030431

Received 4 JUN 2021
Accepted 8 OCT 2021

Author Contributions:
Conceptualization: Zhuangji Wang, Resham Thapa, Dennis Timlin, David Fleisher, Steven Mirsky, Miguel Cabrera, Thomas Sauer, Vangimalla R. Reddy, Robert Horton, Katherine Tully
Formal analysis: Zhuangji Wang, Resham Thapa, Dennis Timlin
Methodology: Zhuangji Wang, Resham Thapa, Dennis Timlin, Sanai Li, Wenguang Sun, Sahila Beegum
Software: Zhuangji Wang, Dennis Timlin, Sanai Li, Wenguang Sun, Sahila Beegum

Abstract Water and thermal dynamics at soil surfaces are influenced by multiple ambient factors, for example, weather, soil, residue mulch, and surface runoff. A surface water and temperature model should address those ambient factors, and their interactions and derivatives. In this study, we developed a process-based simulation model for surface water and heat transfer with two main ambient factors, residue mulch and surface runoff. Surface water content and temperature are simulated with a modified Philip and de Vries (1957) model, including precipitation interception and radiation attenuation in residue mulch. Surface runoff is modeled with the Saint-Venant equation. Residue decomposition, as a derivative, is computed via a modified CERES-N model. Interactions between surface runoff and residue mulch, and dynamic decreases in residue mulch thickness due to decomposition are also included. The model was modularized and deployed with a "layered module architecture" in MAIZSIM, such that the main ambient factors, interactions, and derivatives can be activated or deactivated based on scenarios or user settings. Illustrative examples include non-decomposable residue mulch, surface runoff and mulch decomposition scenarios. Results demonstrate that residue mulch can conserve soil water and reduce temporal variations of surface temperature. Surface runoff and its effects on water infiltration and surface temperature, and nitrogen mineralization during decomposition are also illustrated. The simulated surface temperature, water content, and mulch decomposition results are similar to literature results from field experiments. This study demonstrates the model workability in simulating surface water and temperature dynamics, and the feasibility of synthesizing multiple factors via a modularized model architecture.

Plain Language Summary Knowledge of the impacts on residue mulch and surface runoff on surface soil is important for agricultural field management. We developed a new method to simulate the moisture and thermal regimes on soil surface with residue mulch and/or surface runoff using a computer program. The computer program can also present the surface runoff and residue decomposition. The program can estimate the nitrogen and carbon (organic matter) exchanges between residue mulch and surface soil. This information will be useful to scientists, agricultural managers and consultants.

1. Introduction

The dynamics of water and thermal conditions at soil surfaces are relatively complicated. First, they are scenario dependent. Multiple ambient factors, such as weather, soil properties, residue mulch, surface runoff, and additional field management practices can impact surface water and heat fluxes. For example, for a bare soil surface, evaporation follows the Penman model (Allen et al., 1998), while with surface mulching, either the mulch is impermeable to vapor flow (Ham & Kluitenberg, 1994), or vapor transfer within the mulch must be quantified to compute surface evaporation (Enrique et al., 1999; Findeling, Chanzy, & de Louvigny, 2003). Temperature at a bare soil surface can be determined using a surface energy balance. When surface runoff occurs, however, ponded water can exert direct influences on soil surface temperature, because liquid water has a relatively large heat capacity. Second, the time periods that ambient factors manifest their effects depend on the processes. For example, the variations of wind speed and surface temperature gradients can induce instantaneous effects on evaporation and sensible heat fluxes by altering the dominant

Supervision: Dennis Timlin, David Fleisher, Steven Mirsky, Miguel Cabrera, Thomas Sauer, Vangimalla R. Reddy, Robert Horton, Katherine Tully
Writing – original draft: Zhuangji Wang, Resham Thapa
Writing – review & editing: Dennis Timlin, Sanai Li, Wenguang Sun, Sahila Beegum, David Fleisher, Steven Mirsky, Miguel Cabrera, Thomas Sauer, Vangimalla R. Reddy, Robert Horton, Katherine Tully

flux mechanisms among diffusion, free convection or forced convection over a period of minutes (Novak et al., 2000a, 2000b). Diurnal changes in radiation can produce periodic variations in soil temperature (Horton & Wierenga, 1983), while precipitation (including irrigation, hereafter) can increase soil water content over an hourly period, which may lead to runoff on sloping soil surfaces (Wang et al., 2020). Residue mulch, from crop residues or cover crops, exerts effects on soil surface water and heat fluxes for a monthly period. Therefore, quantification of ambient factors and simulations of soil surface water and heat fluxes should be adaptive to the ambient conditions under appropriate time scales. Third, individual ambient factors can induce derivative processes ("side effects"), while interactions may occur among multiple ambient factors. For example, residue decomposition, which decreases the biomass and the thickness of surface residue mulch with respect to time, can be considered as a derivative process of residue mulch. When runoff occurs on a surface with residue mulch, surface roughness can be increased due to the existence of residue mulch; hence the horizontal momentum of runoff fluxes is reduced (Findeling, Ruy, & Scopel, 2003).

Besides the physical processes mentioned above, to implement numerical simulations of surface water and heat transfer, the soil surface is considered as a thin boundary layer occupied by air near the soil surface, which supports relatively fast vapor and heat exchanges, but has relatively small water and heat capacity. Rapid fluctuations of water and heat fluxes may occur at the soil surface and induce numerical instabilities in computing the water content and temperature near the soil surface. Therefore, to develop a generic process-based model that can simulate water and temperature at soil surfaces, multiple processes such as vapor and heat fluxes, and surface runoff should be included, adjusted, and stabilized adaptively based on ambient factors under a range of time scales. Residue mulch is a commonly used management practice and surface runoff usually occurs in agricultural fields. Therefore, it is useful to include them, as well as their interactions and derivatives [residue decomposition and nitrogen (N) release] in numerical simulations to enhance our understanding of soil surface water and heat dynamics from a modeling perspective.

Residue mulch influences the physical processes at a soil surface in multiple ways. It partially blocks solar radiation, conserves soil water, and mitigates soil temperature variations (Unger, 1994). For example, residue mulch can protect a crop from heat stress by reducing soil surface temperature (Kader et al., 2017), or warm topsoil and benefit seedling emergence in relatively cold regions during early spring (Azooz et al., 1997; Li et al., 2009). Process-based models have been applied to simulate water and heat fluxes for mulched soil surfaces; however, model complexity depends on the simulation goals. When the objective is to investigate soil water and temperature, surface mulch is treated as a boundary condition. For example, Chung and Horton (1987) applied a surface energy balance approach to model soil temperature with or without mulch. Ham and Kluitenberg (1994) expressed the transmission and reflection of shortwave and longwave radiation between the surface soil and mulch as a geometric series. Although Bristow et al. (1986), Sui et al. (1992) and Enrique et al. (1999) applied partial differential equation models to approximate water and heat flows within residue mulch, diffusion was assumed to be the dominant mechanism. In their models, wind speed variations and diffusive fluxes within residue mulch were not explicitly calculated, but were estimated with empirical extinction coefficients. In general, those models successfully predicted a 5%–30% decrease in soil water evaporation, some increases in transpiration, and 1–5°C temperature differences for surface soil with and without mulch.

If the goal is to investigate water potential and temperature within residue mulch, an accurate and explicit description of the physical processes in the surface mulch is required. For example, Chen et al. (1997a) improved the "renewal model" (van Atta, 1977) by introducing a finite micro-front time to the temperature ramp function and adjusting the ramp period by temperature structure functions, which revealed the surface roughness effects on coherent turbulence and temperature fluctuations. Chen et al. (1997b) correlated temperature ramp periods with surface roughness, such that the "renewal model" could estimate sensible heat fluxes for straw mulch under laminar and turbulent conditions. Novak et al. (2000a) characterized the turbulence statistics in straw mulch with small-scale wind speed and temperature measurements, where free convection and turbulence were observed, and an exponential attenuation of mean "cup" wind speed in the straw mulch was also reported. Novak et al. (2000b) combined convective fluxes, radiation, and molecular heat and vapor diffusion to simulate the thermal and water regimes of straw mulch during a wetting-drying cycle and provided energy balance estimations. The studies from Chen et al. (1997a, 1997b) and Novak et al. (2000a, 2000b) required minute-scale measurements of wind speed and temperature.

However, weather condition measurements in agricultural fields are usually performed at hourly or daily scales. Therefore, Findeling, Chanzy, and de Louvigny (2003) proposed "long-distance" convective fluxes of vapor and heat in their TEC_{mulch} model, where the convections were approximated as source-sink terms in the coupled heat and water transfer model without using the turbulence statistics, and the spatial differentiation was only applied to diffusive fluxes. The TEC_{mulch} model (Findeling, Chanzy, & de Louvigny, 2003) design prevented the spatial differentiation of convective fluxes, hence enhancing the numerical stability of the model, while the designs in Chen et al. (1997a, 1997b) and Novak et al. (2000a, 2000b) provided detailed descriptions on the physical processes within residue mulch. Thus, developing a new numerical scheme is needed to leverage the strengths among those designs.

Residue mulch can also reduce solar radiation received at a soil surface, but the radiation attenuation depends on residue types and properties. For example, Novak et al. (2000) proposed a multi-layer model for straw mulch, which used a residue-area index and a clumping index to characterize mulch induced radiation attenuation. Then, a vertical distribution of energy input was determined by summing the shortwave and longwave radiation at pre-defined, internal (virtual) surfaces within residue mulch. In contrast, Findeling, Chanzy, and de Louvigny (2003) applied an opaque model (Chung & Horton, 1987) to compute radiation received at a soil surface under maize residue mulch.

Decomposition is a derivative process of residue mulch application, where the material mass of residue mulch declines, and decomposed materials can serve as a source of soil organic matter. Multiple models have been proposed to simulate the carbon (C) and N dynamics within residue mulch, as well as the exchange of N between residue mulch and surface soil (Wells et al., 2017; Williams et al., 2018). Because water, temperature and microbial activity within residue mulch are not uniformly distributed, decomposition occurring near the mulch-soil interface tends to be faster than decomposition near the mulch-air interface. Such a vertical variation in decomposition rates were described in two perspectives: (a) in APSIM-Residue (Thorburn et al., 2001) and CERES-N (Carley, 2021; Quemada et al., 1997; Thapa, unpublished data), the residue mulch was treated as a single layer, and an empirical contacting factor was introduced to distinguish the actively decomposed portion and the slowly decomposed portion; (b) in EXPERT-N (Berkenkamp et al., 2002) and $PASTIS_{mulch}$ (Findeling et al., 2007), residue mulch was artificially divided into two layers, where the lower layer (the contacting portion) was actively decomposed and the upper layer (the non-contacting portion) transported raw organic matter to the lower layer based on an empirical feeding rate. However, since both perspectives, that is, the contacting factor in (a) and the two-layer division in (b), are characterized by the variation of decomposition rates, the two perspectives are mathematically homological. In addition to residue mulch decomposition and C and N exchanges between residue mulch and surface soil, decomposition can also result in shrinkages of residue mulch thickness, which has not yet been fully considered in the simulations of surface water and temperature. Most of the existing models assume a constant thickness for residue mulch during the simulations (also known as "rigid mulch"). Therefore, it is important to design a model that can simulate water and heat transfer within "shrinking mulch," as well as quantify on the mulch decomposition rates with the simulated mulch temperature and water content.

Surface runoff occurs when precipitation exceeds the infiltrability of the surface soil. The amount of ponded water on a soil surface is quantified based on precipitation and infiltration fluxes (Appels et al., 2011). Horizontal movement of surface runoff can be described via diffusive wave models or the Saint Venant equation (Kollet & Maxwell, 2006; Singh & Bhallamudi, 1998). Residue mulch can increase the surface roughness and pathway tortuosity, hence decrease the horizontal momentum of surface runoff, and potentially increase the ponding depth and the infiltration flux (Findeling, Ruy, & Scopel, 2003; Savabi & Stott, 1994). For example, Findeling, Ruy, and Scopel (2003) defined the surface water capacity and infiltration rate based on mulch biomass, and surface runoff through residue mulch was expressed via the Darcy-Weisbach Law, such that surface roughness can be explicitly expressed as a Darcy friction factor (Gilley et al., 1991). Ruy et al. (2006) and Vieira et al. (2018) applied empirical or physical models (the FDTF, RUSLE, MMF, and PESERA models) to evaluate surface runoff under a variety of mulching conditions. Conversely, surface runoff could also affect water and temperature dynamics in residue mulch by submerging a portion of the residue mulch and changing the underlying surface of the residue mulch from a mulch-soil interface to a mulch-water interface. These kinds of "surface runoff to residue mulch" effects have not yet been fully studied in existing process-based models.

When residue mulch and surface runoff exist, direct measurements of water potential, temperature, and water and heat fluxes at a soil surface are challenging, because (a) residue mulch is a relatively loose material occupying only a relatively thin layer on the soil surface; (b) water and heat fluxes, as well as surface runoff are transient and fluctuate rapidly. Therefore, numerical models become a promising way to study soil surface water and thermal dynamics. The objective of this study is to develop a process-based model for soil surface water and temperature simulations with residue mulch and surface runoff as the two main ambient factors. Water content and temperature distributions in residue mulch and soil along both horizontal and vertical directions are considered; hence this model performs simulations based on a 2-D spatial domain. Interactions between residue mulch and surface runoff, as well as mulch decomposition as a derivative process, are also included. The model should be adaptive to scenarios with or without residue mulch or surface runoff. Processes associated with the two main ambient factors, and their interactions and derivative processes should be developed as independent modules and linked following a "layered module architecture" with a universal expression for vapor and heat fluxes across the mulch-air, mulch-water or mulch-soil interface. MAIZSIM is an integrated simulation package for soil physical and chemical processes and maize development (Kim et al., 2012). The proposed soil surface model developed in this study can be implemented within MAIZSIM to establish a completed Soil-Vegetation-Atmosphere-Transfer (SVAT) modeling framework and provide information on the water content, temperature and nutrition levels on surface soil.

2. Model Development

A process-based model including surface water fluxes (precipitation and evaporation), heat exchanges (conduction and convection), and radiation within residue mulch, that is, straw or cereal rye, is established in Sections 2.1 and 2.2, and it supports simulations of the residue mulch effects on soil surface water and thermal dynamics. Except for scenarios with precipitation and surface runoff, we assume that vapor fluxes through the residue pore-space dominate the water movement within the residue mulch, while liquid water in the solid portion of the residue mulch is in equilibrium with the vapor phase based on water potential. That is because the solid portion of the residue mulch (i.e., the plant tissue) is relatively loose and only occupies a relatively small fraction of the total mulch volume, and solid-solid connections and paths for liquid water flow are relatively weak. Surface runoff and its interaction with residue mulch are presented in Section 2.3. A "layered module architecture" and a dataflow chart are introduced in Section 2.4, which enable the inclusion of multiple ambient factors and processes presented in Sections 2.1–2.3. In Section 2.5, we introduce the decomposition rules and the C and N dynamics within residue mulch. Nitrogen exchange between residue mulch and surface soil, as well as the adaptation of the process-based models in Section 2.1–2.4 to the shrinkage of residue mulch, due to decomposition, are also discussed.

2.1. Coupled Heat and Water Movement in Residue Mulch

The governing equations of water and temperature dynamics within residue mulch can be expressed using a coupled heat and water transfer model (Philip & de Vries, 1957) with adjustments based on the $\mathrm{TEC}_{\mathrm{mulch}}$ model (Findeling, Chanzy, & de Louvigny, 2003).

$$\begin{cases} C_{hh}\dfrac{\partial h}{\partial t} + C_{Th}\dfrac{\partial T}{\partial t} = -\nabla\cdot\left(q_{wd} + q_{wc}\right) + \rho_w\dfrac{\partial}{\partial z}P \\ C_{hT}\dfrac{\partial h}{\partial t} + C_{TT}\dfrac{\partial T}{\partial t} = -\nabla\cdot\left(q_{Td} + q_{Tc} + q_{Tl}\right) + R \end{cases} \tag{1}$$

In Equation 1, $h\left(\text{unit : m, hereafter}\right)$ and $T\left(\mathrm{K}\right)$ are the matric potential and temperature within residue mulch; $t\left(\mathrm{s}\right)$ is time; $\nabla = \left[\partial_x, \partial_z\right]^T$ represents the gradient with respect to the horizontal dimension $[x \in \left(0, X_M\right), \mathrm{m}]$ and the vertical dimension $[z \in \left(0, Z_M\right), \mathrm{m}]$, where $X_M\left(\text{width}\right) \times Z_M\left(\text{thickness}\right)$ is the spatial scale of the residue mulch. The symbol "·" indicates the inner product between vectors; therefore, "$\nabla\cdot$" becomes the divergence operator. $q_{wd}\left(\mathrm{g\ m^{-2}\ s^{-1}}\right)$ and $q_{wc}\left(\mathrm{g\ m^{-2}\ s^{-1}}\right)$ are conductive and convective vapor fluxes; $q_{Td}\left(\mathrm{J\ m^{-2}\ s^{-1}}\right)$, $q_{Tc}\left(\mathrm{J\ m^{-2}\ s^{-1}}\right)$, and $q_{Tl}\left(\mathrm{J\ m^{-2}\ s^{-1}}\right)$ are conductive, convective, and latent heat fluxes. In the $\mathrm{TEC}_{\mathrm{mulch}}$ model, q_{Tl} is implicitly merged into q_{Tc} (see Equation 7b in Findeling, Chanzy, &

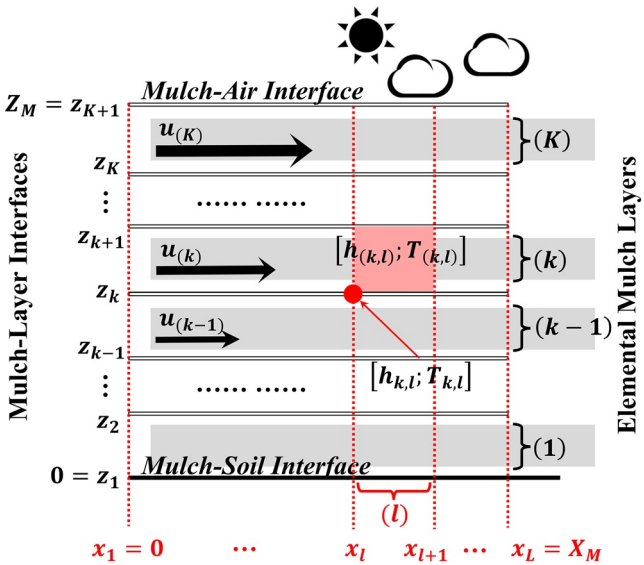

Figure 1. A spatial grid of residue mulch. Along the vertical dimension, the residue mulch is discretized into (K) elemental layers with K+1 mulch-layer interface; along the horizontal dimension, the residue mulch is discretized into (L) elements with L+1 nodes. Wind speed (u) in each elemental layer is presented. For physical properties, such as h, T, and u, parenthesized subscripts are used element-wisely, and non-parenthesized subscripts are used node-wisely, for example, $\left[h_{(k,l)}; T_{(k,l)}\right]$ is an element-wise representation, $\left[h_{k,l}; T_{k,l}\right]$ is a node-wise representation. Mixed subscripts, $\left[h_{(k),l}; T_{(k),l}\right]$ indicates the h, T values for the elemental layer (k) at position $x = x_l$ and $\left[h_{k,(l)}; T_{k,(l)}\right]$ indicates the h, T values for the horizontal element (l) at mulch-layer interface $k\,(z = z_k)$. Both representations will be used in model establishment.

de Louvigny, 2003). In this study, however, q_{Tl} is expressed explicitly in Equation 1 to include latent heat carried by both conductive and convective vapor fluxes. $P\left(\mathrm{m\ s^{-1}}\right)$ and $R\left(\mathrm{W\ m^{-2}}\right)$ indicate the water input by precipitation and the energy input by radiation. $\rho_w \approx 1.0\times10^6\left(\mathrm{g\ m^{-3}}\right)$ is the liquid water density.

C_{hh}, C_{Th}, C_{hT} and C_{TT} in Equation 1 are the coefficients related to the water and heat capacity of residue mulch, which are calculated similar to those for soil (Wang et al., 2017). The differences in the expressions of C_{hh}, C_{Th}, C_{hT} and C_{TT} between soil and residue mulch follows (a) residue mulch usually has relatively low volumetric water content, and (b) the assumption that vapor flux is the dominant mechanism of water flow within mulch pore spaces, when no precipitation or surface runoff occurs. The relatively low volumetric water content is because the liquid water, within the plant residue, occupies only a small fraction of the total mulch volume, and a relatively large fraction of the mulch volume is air-filled; however, if water content within residue mulch is expressed based on gravimetric water content, it can achieve a relatively large number based on the mass of plant residue and the ambient humidity.

$$\begin{cases} C_{hh} = \rho_w \dfrac{\partial\theta}{\partial h} + \varphi_m \rho_{v,s} H_r \dfrac{\partial H_r}{\partial h} \\ C_{Th} = \varphi_m \left[H_r \dfrac{\partial \rho_{v,s}}{\partial T} + \rho_{v,s} \dfrac{\partial H_r}{\partial T} \right] \\ C_{hT} = \varphi_m \rho_{v,s} H_r \left[C_{v,v} + C_{v,s}\left(T - T_{\mathrm{ref}}\right) \right] \dfrac{\partial H_r}{\partial h} + C_{w,s}\rho_w \left(T - T_{\mathrm{ref}}\right) \dfrac{\partial\theta}{\partial h} \\ C_{TT} = \left[C_{w,s}\rho_w\theta + C_{m,s}\rho_m + \varphi_m \left(C_{a,s}\rho_a + C_{v,s}\rho_{v,s} H_r \right) \right] \\ \qquad + \varphi_m \left[C_{v,v} + C_{v,s}\left(T - T_{\mathrm{ref}}\right) \right] \cdot \left[H_r \dfrac{\partial \rho_{v,s}}{\partial T} + \rho_{v,s} \dfrac{\partial H_r}{\partial T} \right] \end{cases} \tag{2}$$

In Equation 2, $\rho_{v,s}\left(\mathrm{g\ m^{-3}}\right)$ is the saturated water vapor density, as a function of T; $\rho_a\left(\mathrm{g\ m^{-3}}, \rho_a \approx 1204.0 \text{ at } 293.75\mathrm{K} \text{ and } 101\,\mathrm{kPa}\right)$ is the dry air density; $\rho_m\left(\mathrm{g\ m^{-3}}\right)$ is the residue mulch density; $\theta\left(\mathrm{m^3 m^{-3}}\right)$ is the mulch volumetric water content; $\varphi_m\left(\mathrm{m^3\ m^{-3}}\right)$ is the mulch porosity; H_r is the mulch relative humidity; $C_{v,v} \approx 2450.0\left(\mathrm{J\ g^{-1}}\right)$ is the heat of vapourization of water; $C_{v,s} \approx 1.862\left(\mathrm{J\ g^{-1}\ K^{-1}}\right)$ is the specific heat of vapor; $C_{w,s} \approx 4.186\left(\mathrm{J\ g^{-1}\ K^{-1}}\right)$ is the specific heat of liquid water; $C_{m,s}\left(\mathrm{J\ g^{-1}\ K^{-1}}\right)$ is the specific heat of residue material; $C_{a,s} \approx 0.718\left(\mathrm{J\ g^{-1}\ K^{-1}}\right)$ is the specific heat of dry air; $T_{\mathrm{ref}}\left(\mathrm{K}\right)$ is an arbitrarily defined reference temperature (for mulch simulations, we can choose $T_{\mathrm{ref}} \approx 293\,\mathrm{K}$).

Equation 1 can be solved with a mixed-hybrid finite element scheme (Chavent & Roberts, 1991). In the numerical implementation, residue mulch is divided into (K) elemental layers, corresponding to $K+1$ mulch-layer interfaces, labeled from the mulch-soil interface at the bottom ($z = 0$) to the mulch-air interface at the top ($z = Z_M$). By combining the elemental layers and an additional horizontal discretization, a 2-D grid for residue mulch can be established. Hereafter, parenthesized subscripts are used for elemental layers or elements with a certain area, for example, $\left[h_{(k,l)}; T_{(k,l)}\right]$ represent matric potential and temperature in element (k,l); non-parenthesized subscripts are used for nodes, for example, $\left[h_{k,l}; T_{k,l}\right]$ represent matric potential and temperature at node (k,l); mixed subscripts are used to refer to a line segment with a certain length, for example, $\left[h_{k,(l)}; T_{k,(l)}\right]$ represent matric potential and temperature within a horizontal element (l) at a mulch-layer interface $k\,(z = z_k)$; while $\left[h_{(k),l}; T_{(k),l}\right]$ represent matric potential and temperature within an elemental layer (k) at a horizontal position $x = x_l$. Both representations will be used in model establishment. An illustrative diagram for the definition of the 2-D grid and the notations is shown in Figure 1.

The wind speed distribution among the elemental layers is required to formulate convective vapor and heat fluxes. When weather datasets are provided at an hourly or daily time scale, direct computation of turbulence statistics is challenging; hence, a vertical distribution of mean wind speed is adopted and expressed as follows (Novak et al., 2000a),

$$\begin{cases} u_* = \dfrac{k_K u_{\text{ref}}}{\ln\left[\left(z_u - d\right)/z_r\right]} \\ u_{(k)} = 0.21 u_* \exp\left(\dfrac{2.2}{Z_m} \times \dfrac{z_k + z_{k+1}}{2}\right) \end{cases} \tag{3}$$

In the first equation, $u_{\text{ref}}\left(\text{m s}^{-1}\right)$ represents the wind speed measured above the mulch-air interface [at a reference height $z_{\text{ref}}\left(\text{m}\right)$, generally at 200 cm above soil surface]; $u_*\left(\text{m s}^{-1}\right)$ is the friction velocity; $k_K = 0.4$ is the von Karman's constant; $d \approx 0.87 \times Z_M\left(\text{m}\right)$ is the surface displacement; $z_r \approx 0.079 \times Z_M\left(\text{m}\right)$ is the roughness length. Differencing from the diabatic wind profile (Campbell & Norman, 1998), the momentum correction factor is omitted to avoid (a) the requirements of high frequency wind speed and temperature measurements, and (b) the iterations in calculating the Monin-Obukhov length. Such a simplification produces reasonable results for the wind speed distribution within residue mulch. The second equation is a numerical description of the mean wind speed in residue mulch, where mean wind speed attenuates exponentially from the mulch-air interface to mulch-soil interface.

Rayleigh number (Ra) and Richardson number (Ri) are two dimensionless quantities that relate the mulch temperature and wind speed to the mechanisms of vapor and heat fluxes, and they can be calculated based on the mulch temperature regime and the wind speed distribution given in Equation 3.

$$\begin{cases} \text{Ra}_{(l)} \underline{\underline{\text{def}}} \dfrac{g\left|\Delta T\right|\left(\Delta z\right)^3}{\bar{T}\nu D_{hm}} = \dfrac{2g\left|T_{(K,l)} - T_{(1,l)}\right| Z_M^3}{\left(T_{(K,l)} + T_{(1,l)}\right)\nu D_{hm}} \\ \text{Ri}_{(l)} \underline{\underline{\text{def}}} \dfrac{g\left|\Delta T\right|\Delta z}{\bar{T}\left(\Delta u\right)^2} = \dfrac{2g\left|T_{(K,l)} - T_{(1,l)}\right| Z_M}{\left(T_{(K,l)} + T_{(1,l)}\right)\left(u_{(K)} - u_{(1)}\right)^2} \end{cases} \tag{4}$$

The "$\underline{\underline{\text{def}}}$" of the two equations indicates definitions of Ra and Ri, while the " $=$ " indicates the calculation methods based on the discretized grid in Figure 1. $\nu \approx 1.5 \times 10^{-5}\left(\text{m}^2\text{s}^{-1}\right)$ is the kinematic viscosity of air; $D_{hm} \approx 2.2 \times 10^{-5}\left(\text{m}^2\ \text{s}^{-1}\right)$ is the molecular thermal diffusivity; $g \approx 9.81\left(\text{m s}^{-2}\right)$ is the gravitational acceleration. "Δ" represents the finite difference; the overline indicates the average. Based on Equation 4, Ra emphasizes the temperature differences, and it serves as a measure for the transition between diffusion and convection. Ri, which is equal to the ratio between Grashof number (Gr) and the square of Reynolds number (Re), characterizes free convection versus forced convection by emphasizing the "shearing force" due to wind speed differences. A relatively large Ri corresponds to a relatively small Re, when free convection dominates the fluxes; a relatively small Ri corresponds to a relatively large Re, when forced convection becomes the main flux mechanism. A summary for the critical values of Re and Ri (Findeling, Chanzy, & de Louvigny, 2003; Novak et al., 2000a) and the associated flux forms is shown in Equation 5. In numerical implementation, Ra and Ri are computed for the whole residue mulch rather than for individual elemental layers. The first reason is that in early studies, Ra and Ri were presented for the whole residue mulch layer (Findeling, Chanzy, & de Louvigny, 2003; Novak et al., 2000a). The second reason is that in the discretized grid, as $\Delta z \to 0$, that is, the thickness of each elemental layer tends to 0, the temperature and wind speed differences between two adjoined elemental layers will be smaller than those differences between the mulch-soil interface and the mulch-air interface, based on Equation 3. Hence, if Ra and Ri are computed for individual elemental layers, they cannot appropriately characterize the diffusive and convective fluxes for the whole residue mulch, since Ra and Ri are functions of temperature and wind speed differences.

$$\begin{cases} \mathrm{Ra} < 1706 \;\Rightarrow\; \text{Diffusion Only}\left(\text{Eq.}\left[6\right]\right) \\ \mathrm{Ra} \geq 1706 \;\Rightarrow\; \begin{cases} \mathrm{Ri} \geq 1 \;\Rightarrow\; \text{Diffusion and Free Convection}\left(\text{Eqs.}\left[6\right],\left[7\right]\right) \\ \mathrm{Ri} < 1 \;\Rightarrow\; \text{Diffusion and Forced Convection}\left(\text{Eqs.}\left[6\right],\left[8\right]\right) \end{cases} \end{cases} \tag{5}$$

Molecular diffusion is used to approximate the diffusive vapor and heat fluxes. A continuous form of diffusive fluxes, expressed using vapor density and temperature gradients, is given in Equation 6.

$$\begin{cases} q_{wd} = -\left[D_v\left(\dfrac{T}{273.15}\right)^{1.75}\varphi_m\Omega_{\text{tort}}\right]\times\nabla\left(\rho_{v,s}H_r\right) \\ q_{Td} = -\left[\underbrace{D_{hm}C_{a,s}\rho_a}_{\substack{\text{thermal conductivity of}\\ \text{air within mulch pores}}} + \underbrace{D_{\boldsymbol{m}}\left(1-\varphi_m\right)}_{\substack{\text{thermal conductivity of}\\ \text{mulch residue solid}}}\right]\times\nabla T \end{cases} \tag{6}$$

In Equation 6, $D_v\left(\mathrm{m^2\ s^{-1}}\right)$ is the vapor diffusivity observed at $293.15\left(\mathrm{K}\right)$ and $101\left(\mathrm{kPa}\right)$, and its value ranges from 2.29×10^{-5} (Kimball et al., 1976) to 2.40×10^{-5} (Campbell & Norman, 1998). $\Omega_{\text{tort}} = \varphi_m^{2/3}$ is the dimensionless tortuosity factor in residue mulch (Lai et al., 1976). We use the total mulch porosity φ_m, instead of the air-filled porosity, to estimate Ω_{tort}, because residue mulch has relatively large porosity and most of the pores are air-filled. The total heat flux is a sum of conductive heat transfers through the air within the mulch pores and the solid portion of residue mulch, where $D_m\left(\mathrm{J\ m^{-1}\ K^{-1}\ s^{-1}}\right)$ is the thermal conductivity for the solid mulch residue tissues.

Convective heat and vapor fluxes are given in Equations 7 and 8. Instead of using the vapor density gradient and temperature gradient, the convective fluxes rely on mass flows caused by the instability of the air within mulch pores. Therefore, the fluxes are not expressed in continuous and differential formulations, but in discretized forms based on the finite differences of vapor pressure or temperature.

$$\begin{cases} C_w^{\text{fr}} = \alpha_{\text{c}}^{\text{fr}}\sqrt{\left|\Delta T\right|}\dfrac{M_{\text{H}_2\text{O}}}{R_g\bar{T}}; \quad q_{wc} = -C_w^{\text{fr}}\Delta\left(P_{v,s}H_r\right) \\ C_h^{\text{fr}} = \alpha_{\text{c}}^{\text{fr}}\sqrt{\left|\Delta T\right|}C_{a,s}\rho_a; \quad q_{Tc} = -C_h^{\text{fr}}\Delta T \end{cases} \tag{7}$$

In Equation 7, C_w^{fr} and C_h^{fr} are the free convective conductance of vapor and heat; $\alpha_{\text{c}}^{\text{fr}} \approx 5.6\times10^{-3}\left(\mathrm{m\ K^{-1/2}\ s^{-1}}\right)$ is an empirical coefficient (Findeling, Chanzy, & de Louvigny, 2003; Novak et al., 2000a); $M_{\text{H}_2\text{O}} \approx 18.02\ \mathrm{g\ mol^{-1}}$ is the molecular weight of water; $R_g \approx 8.314\left(\mathrm{J\ mol^{-1}\ K^{-1}}\right)$ is the gas constant; $P_{v,s}\left(\mathrm{Pa}\right)$ is the saturated vapor pressure in residue mulch. Δ represents the finite difference. $\bar{T}$ indicates the average temperature of the two ending-points for vapor and heat flows (i.e., two adjoined elements in Figure 1).

$$\begin{cases} C_w^{\text{fo}} = 0.155\times k_K^2 u\dfrac{M_{\text{H}_2\text{O}}}{R_g\bar{T}}; \quad q_{wc} = -C_w^{\text{fo}}\Delta\left(P_{v,s}H_r\right) \\ C_h^{\text{fo}} = 0.155\times k_K^2 u C_{a,s}\rho_a; \quad q_{Tc} = -C_h^{\text{fo}}\Delta T \end{cases} \tag{8}$$

Equation 8 shares a form similar to Equation 7. C_w^{fo} and C_h^{fo} are the forced convective conductance of vapor and heat. The coefficient $0.155 \approx \left[\ln 0.079\right]^{-2}$, where 0.079 is the coefficient of surface roughness length $\left(z_r\right)$ in Equation 3. Comparing Equations 7 and 8 with the ones in $\text{TEC}_{\text{mulch}}$ model, the exponential dependence of the empirical extinction coefficient (see χ in Findeling, Chanzy, & de Louvigny, 2003) is excluded because the wind speed attenuation and the temperature variations in residue mulch are already considered. Furthermore, the active mulch area density (see ξ_m in Findeling, Chanzy, & de Louvigny, 2003) is eliminated since the convective fluxes are written into the spatial differentiations in Equation 1, instead of being treated as "long-distance" source-sink terms.

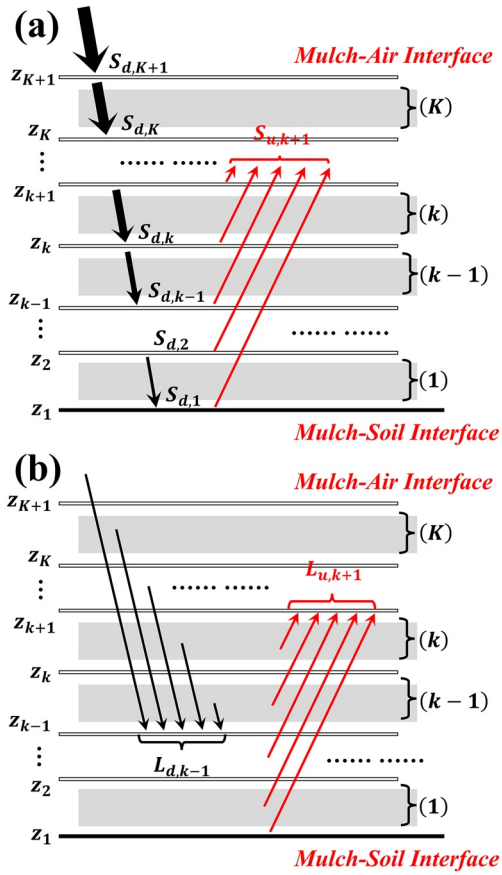

Figure 2. (a) Shortwave radiation and (b) longwave radiation within the mulch residue. The vertical discretization of the mulch follows Figure 1. Example radiation values at specific interfaces, such as $S_{d,k}$ and $S_{u,k+1}$ for shortwave radiation (a), as well as $L_{d,k-1}$ and $L_{u,k+1}$ for longwave radiation (b), are presented.

Latent heat flux represents the heat carried by the vapor transfer within residue mulch. The amount of energy transported by a unit mass of vapor can be determined by the difference in internal energy between the vapor at current temperature (T) and the liquid water at reference temperature (T_{ref}), as expressed in Equation 9. Based on the up-wind scheme, T from the upstream direction of $(q_{wd} + q_{wc})$ should be used to determine the latent heat flux.

$$q_{Tl} = (q_{wd} + q_{wc})\underbrace{\left[C_{v,v} + C_{v,s}(T - T_{\text{ref}})\right]}_{\text{The internal energy of vapor, refer to } T_{\text{ref}}} \tag{9}$$

2.2. Precipitation Interception and Radiation Attenuation Within the Residue Mulch

In Equation 1, precipitation $\left[P\left(\text{m s}^{-1}\right)\right]$ is converted to a mass unit using ρ_w. Because of mulch interception, the P value decreases from the mulch-air interface to the mulch-soil interface, represented by the partial differentiation along the vertical direction, that is, $\frac{\partial}{\partial z}P$. Since the vertical dimension is discretized into elemental layers, precipitation intercepted by a given elemental layer can be determined using the precipitation intensity received and the water absorbed at that elemental layer. Findeling, Chanzy, and de Louvigny (2003) assumed that the maximum water absorbed at each elemental layer was equal to the porosity; while in this study, we assume the maximal amount of water absorbed is based on vapor-pressure deficit. The actual water absorption should be within the range of the two assumptions; unfortunately, observed values of precipitation interception by residue mulch are rarely reported. The intercepted precipitation is considered as the water input for that elemental layer, while the bypassed portion becomes the amount of precipitation received by the lower elemental layer. Precipitation interception can be computed using a recursive relation from the mulch-air interface to the mulch-soil interface, that is,

$$\begin{cases} P_{(k,l)} = \max\left\{\dfrac{\rho_{v,s}(1 - H_r)(z_{k+1} - z_k)}{\rho_w \Delta t}, P_0\right\} \\ P_0 \leftarrow P_0 - P_{(k,l)}, \quad k = K, K-1, \ldots, 1 \end{cases} \tag{10}$$

In Equation 10, Δt is the time step used to solve Equation 1. $P_0\left(\text{m s}^{-1}\right)$ is initialized as the precipitation received from the atmosphere, and the recursive process is performed from elemental layer (K) to elemental layer (1). For element (k,l), $P_{(k,l)}$ is taken from P_0 as the amount of water adsorbed, and the remaining portion, that is, $P_0 - P_{(k,l)}$, is assigned as the precipitation received by the element $(k-1,l)$, until the total amount of precipitation is exhausted, or the precipitation reaches the mulch-soil interface. "←" represents "assignment" hereafter.

Radiation $\left[R\left(\text{W m}^{-2}\right)\right]$ is expressed as a source-sink term in Equation 1. A multi-layer model proposed by Novak et al. (2000) is adopted to simulate the radiation attenuation within residue mulch, and illustrative diagrams are shown in Figure 2. Radiation reaching the mulch-air interface is divided into the shortwave portion and the longwave portion. The upward or downward radiation is calculated separately at each mulch-layer interface. The multi-layer model is originally defined in 1-D space, along the vertical dimension. Such a model can be easily extended to a 2-D grid, where the 1-D model is applied within each of the horizontal elements.

Figure 2a presents the downward shortwave radiation and its upward reflection. The attenuation of downward shortwave radiation follows a geometrical pattern proposed by Ross (1976), that is,

$$S_{d,k} = \begin{cases} S_0 & \text{if} \quad k = K+1 \\ S_0\left(1-\Delta R\right) & \text{if} \quad k = K \\ \underbrace{S_0\left(1-\Delta R\right)\left(1-\Omega_{\text{cf}}\Delta R\right)^{K-k}}_{=\tau_{K-k+1}} & \text{if} \quad k = 1,2,\ldots,K-1 \end{cases} \tag{11}$$

In Equation 11, $S_0\left(\text{W m}^{-2}\right)$ is the solar irradiance above the mulch-air interface; ΔR is the residue-area index; Ω_{cf} is the clumping index associated with residue arrangement; $\tau_n \underline{\underline{\text{def}}} \left(1-\Delta R\right)\left(1-\Omega_{\text{cf}}\Delta R\right)^{n-1}$ is the transmissivity through n consecutive elemental layers. For the upward shortwave reflection across a given mulch-layer interface, for example, $k+1$ in Figure 2a, the reflected radiation from the given interface, as well as all of the interfaces beneath, should be accumulated, that is,

$$S_{u,k} = \begin{cases} S_{d,1}\alpha_s & \text{if} \quad k = 1 \\ S_{d,1}\alpha_s\left(1-\Delta R\right) + \alpha_m\left(S_{d,2} - S_{d,1}\right) & \text{if} \quad k = 2 \\ \underbrace{S_{d,1}\alpha_s\tau_{k-1}}_{\substack{\text{mulch-soil} \\ \text{surface}}} + \underbrace{\alpha_m \sum_{j=2}^{k-1}\left(S_{d,j} - S_{d,j-1}\right)\tau_{k-j}}_{\text{mulch-layer interfaces beneath}} + \underbrace{\alpha_m\left(S_{d,k} - S_{d,k-1}\right)}_{\substack{\text{the given mulch-layer} \\ \text{interface}}} & \text{if} \quad k = 3,4,\ldots,K+1 \end{cases} \tag{12}$$

In Equation 12, α_m is the shortwave reflectivity of residue mulch and α_s is the shortwave reflectivity of soil surface.

Figure 2b presents downward and upward longwave radiation. Longwave radiation from the atmosphere, residue mulch or surface soil follows the Stefan-Boltzmann Law. Given a mulch-layer interface, for example, $k-1$ in Figure 2b, for each horizontal element, the downward radiation received at that mulch-layer interface accumulates all of the downward longwave radiation generated from the mulch elements above, including the atmosphere, that is,

$$L_{d,k,(l)} = \begin{cases} \varepsilon_a\sigma T_a^4 & \text{if} \quad k = K+1, l = 1,2,\ldots,L \\ \varepsilon_a\sigma T_a^4\tau_1 + \varepsilon_m\sigma T_{(K,l)}^4\left[1-\tau_1\right] & \text{if} \quad k = K, l = 1,2,\ldots,L \\ \underbrace{\varepsilon_a\sigma T_a^4\tau_{K-k+1}}_{\text{atmosphere}} + \underbrace{\varepsilon_m \sum_{j=k+1}^{K}\sigma T_{(j,l)}^4\left[\tau_{j-k} - \tau_{j-k+1}\right]}_{\substack{\text{mulch elemental layers above} \\ \text{(not include the adjoined one)}}} + \underbrace{\varepsilon_m\sigma T_{(k,l)}^4\left[1-\tau_1\right]}_{\substack{\text{mulch elemental layer} \\ \text{adjoined to the given} \\ \text{mulch-layer interface}}} & \text{if} \quad k = 1,2,\ldots,K-1, l = 1,2,\ldots,L \end{cases} \tag{13}$$

In Equation 13, $T_a\left(\text{K}\right)$ is the atmosphere temperature at z_{ref} (an isothermal air layer between mulch-air interface and z_{ref} is assumed), while $T_{(k,l)}, k = 1,2,\ldots,K; l = 1,2,\ldots L$ is the element-wise temperature within the residue mulch. ε_a and ε_m are longwave emissivity of the atmosphere and residue mulch, where $\varepsilon_a \approx \left(1-0.84C\right)\left[0.6 + 5.95\times10^{-3}P_{v,s}H_r\exp\left(1500\,/\,T_a\right)\right] + 0.84C$, with C as the cloud factor (Bristow et al., 1986; Novak & Black, 1985). $\sigma \approx 5.67\times10^{-8}$ W m^{-2} K^{-4} is the Stefan-Boltzmann constant. Similarly, the upward longwave radiation reaches each horizontal element at a given mulch-layer interface, for example, $k+1$ in Figure 2b, should include all of the longwave radiation generated from mulch elements below, as well as the soil surface, that is,

$$L_{u,k,(l)} = \begin{cases} \varepsilon_s\sigma T_s^4 & \text{if} \quad k = 1, l = 1,2,\ldots,L \\ \varepsilon_s\sigma T_s^4\tau_1 + \varepsilon_m\sigma T_{(1,l)}^4\left[1-\tau_1\right] & \text{if} \quad k = 2, l = 1,2,\ldots,L \\ \underbrace{\varepsilon_s\sigma T_s^4\tau_k}_{\substack{\text{surface} \\ \text{soil}}} + \underbrace{\varepsilon_m \sum_{j=1}^{k-2}\sigma T_{(j,l)}^4\left[\tau_{k-j-1} - \tau_{k-j}\right]}_{\substack{\text{mulch elemental layers below} \\ \text{(not include the adjoined one)}}} + \underbrace{\varepsilon_m\sigma T_{(k-1,l)}^4\left[1-\tau_1\right]}_{\substack{\text{mulch elemental layer} \\ \text{adjoined to the given} \\ \text{mulch-layer interface}}} & \text{if} \quad k = 3,4,\ldots,K+1, l = 1,2,\ldots,L \end{cases} \tag{14}$$

$\varepsilon_s \approx 1$ and T_s are the longwave emissivity and the temperature of the soil surface. Based on Equations 11–14, the net radiation flux across a given mulch-layer interface is the sum of all the shortwave and longwave components, and the net radiation energy received by each element is the difference of the net radiation

flux received at the upper interface and lower interface of the element, which is presented in Equation 15 using the parenthesized or mixed subscripts introduced in Figure 1.

$$\begin{cases} R_{\mathrm{net},k,(l)} = S_{d,k} - S_{u,k} + L_{d,k,(l)} - L_{u,k,(l)}, & k = 1,2,\ldots,K+1, l = 1,2,\ldots,L \\ R_{(k,l)} = R_{\mathrm{net},k,(l)} - R_{\mathrm{net},k+1,(l)}, & k = 1,2,\ldots,K, l = 1,2,\ldots,L \end{cases} \tag{15}$$

2.3. Surface Runoff Model

The Saint-Venant equation is adopted as the governing model for surface runoff, which is an integral average of the Navier-Stokes equation with respect to ponded water depth. In Equation 16, the first equation represents the conservation of mass for the ponded water; the second equation represents the conservation of momentum for the runoff flux.

$$\begin{cases} \dfrac{\partial \tilde{h}}{\partial t} = -\dfrac{\partial q}{\partial l} + \left(\tilde{P} - \tilde{I}\right) \\ \dfrac{\partial q}{\partial t} = -\dfrac{\partial}{\partial l}\left(\dfrac{q^2}{\tilde{h}} + \dfrac{g\tilde{h}^2}{2}\right) + g\tilde{h}\left(S_0 - S_f\right) \end{cases} \tag{16}$$

$\tilde{h}\left(\mathrm{m}\right)$ is the ponding depth of surface liquid water; $q\left(\mathrm{m^2 s^{-1}}\right)$ is the runoff flux; S_0 and $S_f = \left(nq\right)^2 / \tilde{h}^{10/3}$ are surface and friction slopes, with $n\left(\mathrm{m^{-1/3}\ s}\right)$ as the Manning roughness. $\partial/\partial l$ represents the partial derivative along the surface slope $\left(l\right)$. $\tilde{P}\left(\mathrm{m\ s^{-1}}\right)$ is the precipitation received on the ponded water surface, which is not necessarily equal to the precipitation from the atmosphere due to the interception by residue mulch. $\tilde{I}\left(\mathrm{m\ s^{-1}}\right)$ represents the infiltration at the soil surface. A numerical solver of Equation 16 has been proposed and implemented by Wang et al. (2020).

Ponded water influences coupled heat and water transfer in residue mulch following two possible ways. (a) Residue mulch can be partially submerged by the ponded water, and only the unsubmerged portion satisfies Equation 1; therefore, the discretized grid in Figure 1 is adjusted based on the ponding depth, and the underlying surface of residue mulch is changed from a mulch-soil interface to a mulch-water interface. (b) The soil surface boundary condition can be changed, that is, when ponded water exists, the water flux changes from evaporation to infiltration, and the soil surface temperature is assumed to be equal to the ponded water temperature.

In the numerical implementation, for (a), a partially submerged residue mulch is assumed, and the grid in Figure 1 is maintained but the mulch-soil interface is moved upwards as a mulch-water interface based on the ponding depth. Therefore, the "effective mulch thickness," that is, the unsubmerged portion, shrinks, and the attenuation of radiation and wind speed, as well as the precipitation interception are computed based on the unsubmerged portion of the grid. However, the original grid is kept in this case, because after the ponded water is drained, Equation 1 should be solved for the whole residue mulch. Note that we avoid the scenario that the ponding depth is larger than the residue mulch thickness, because once the residue mulch is totally submerged, its effects on regulating surface water and temperature will disappear, and the residue mulch may float and detach from the soil surface. That scenario can be eliminated in numerical simulations by pre-specifying a maximum ponding depth that the surface residue mulch can hold, which is smaller than the mulch thickness based on Findeling, Ruy, and Scopel (2003) (e.g., half of the total mulch thickness is assumed in Section 3). For (b), the temperature of the ponded water is assumed to be equal to the air temperature, because precipitation from the atmosphere is the main source of the ponded water.

Water fluxes at the soil surface are implemented based on a continuous time boundary condition, associated with the Richards equation (Kouznetsov, 1989; Wang et al., 2020), that is,

$$\frac{\partial(\eta\left(h\right) \times h)}{\partial t} - \left(\tilde{P} - \tilde{I}\right) = 0 \tag{17}$$

In Equation 17, $h\left(\mathrm{m}\right)$ represents the water potential near the soil surface, rather than the water potential of residue mulch in Equation 1; $\eta\left(h\right)$ is the Heaviside step function. When ponded water exists, $h \geq 0$ and

$\eta(h) = 1$ due to the pressure potential; when ponded water is drained, $h < 0$ and $\eta(h) = 0$. Therefore, Equation 17 can be automatically activated or deactivated based on the existence of ponded water to switch the water fluxes between infiltration and evaporation.

2.4. Model Implementation and Dataflow Control

Models established in Sections 2.1–2.3 are implemented in MAIZSIM, a modular-based soil-crop simulator including multiple soil physical and chemical processes (via MAIZSIM sub-model "2DSOIL," Timlin et al., 1996), as well as maize growth and soil-plant interactions (via a crop sub-model in MAIZSIM, Kim et al., 2012; Wang et al., 2021). With proper modifications in the crop sub-model, variations of MAIZSIM can be extended for other crops, for example, SPUDSIM for potato (Fleisher et al., 2020) or an updated GLYCIM for soybean (Sun et al., 2021). Climate factors, crop growth, agricultural management including fertilizer and irrigation, and soil water, heat and solute transfer are coded as separated modules. The management of public variables in MAIZSIM facilitates efficient data exchanges among modules; while local variables and subroutines within each module are processed privately (Timlin et al., 1996). Therefore, modules in MAIZSIM can be included, excluded, or updated with minimal modifications on other modules.

Models in Sections 2.1–2.3 are coded into two modules. To ensure the generality, a "layered module architecture" is introduced and shown in Figure 3, where the "Residue Mulch Module," "Surface Runoff Module" and "Soil Physical and Chemical Models" are considered as three layers. Variables related to surface water properties, that is, the "Water Fluxes Group," and thermal properties, that is, the "Thermal Fluxes Group," contain the mass and energy boundary conditions between soil and atmosphere. They are first computed based on soil and weather conditions. Then, the "Water Fluxes Group" and "Thermal Fluxes Group" are sequentially modified by the "Residue Mulch Module" and the "Surface Runoff Module." If residue mulch or surface runoff does not exist, the corresponding module layer will be bypassed automatically, and the values in the "Water Fluxes Group" and "Thermal Fluxes Group" will remain unchanged. The advantages of using the "layered module architecture" are that (a) models in individual layers can be activated or deactivated with minimal effects on other layers, hence MAIZSIM can be easily transformed among multiple scenarios, that is, with or without residue mulch, with or without surface runoff; (b) if additional surface processes or management practices occur, we only need to develop additional modular layers to this architecture without changing the existing data flow chart.

To optimize the model accuracy and numerical stability, each layer in the "layered module architecture" defines its own local time step. The vapor and heat fluxes in residue mulch may fluctuate rapidly under a relatively small time scale; hence a relatively small time step is required. However, water and heat fluxes in soil are relatively slow and soil has a relatively large buffering capacity for the changes in water potential and temperature, such that a relatively large time step can be adopted. In the proposed "layered module architecture" (Figure 3), the local time step in Layer 3 (soil) is treated as the global step, which also governs the time advancement for the whole MAIZSIM model. Modules in Layer 1 (residue mulch) and Layer 2 (ponded water) subdivide the global step as their local steps, based on numerical stability criteria. Therefore, for one global step in Layer 3, computation for more than one local step can be performed in Layer 1 and Layer 2. Local time recorders in Layer 1 and Layer 2 are defined to accumulate their local time steps, until those time recorders achieve one global step in Layer 3. During the multiple iterations in Layer 1 and Layer 2, variables in Layer 3, such as soil water potential and temperature, are assumed to be constant. After one global step, the local time recorded in all the layers can be automatically aligned to the global time in MAIZSIM.

2.5. Residue Mulch Decomposition and Influences on the Water and Temperature Model

Multiple factors control residue mulch decomposition and N mineralization, including (a) residue biochemical composition, that is, N concentration, carbon-nitrogen ratio (C/N ratio) and mass fractions of carbohydrate (CARB), (holo/hemi)-cellulose (CELL) or lignin (LIGN), (b) agricultural management, for example, tillage, (c) weather conditions, and (d) the activity of decomposer communities, for example, fungi or bacteria (Cabrera et al., 2005; Poffenbarger et al., 2015; Vigil & Kissel, 1991; Wagger et al., 1998). Conversely, residue decomposition and N mineralization also change mulch quality, for example, C/N ratio.

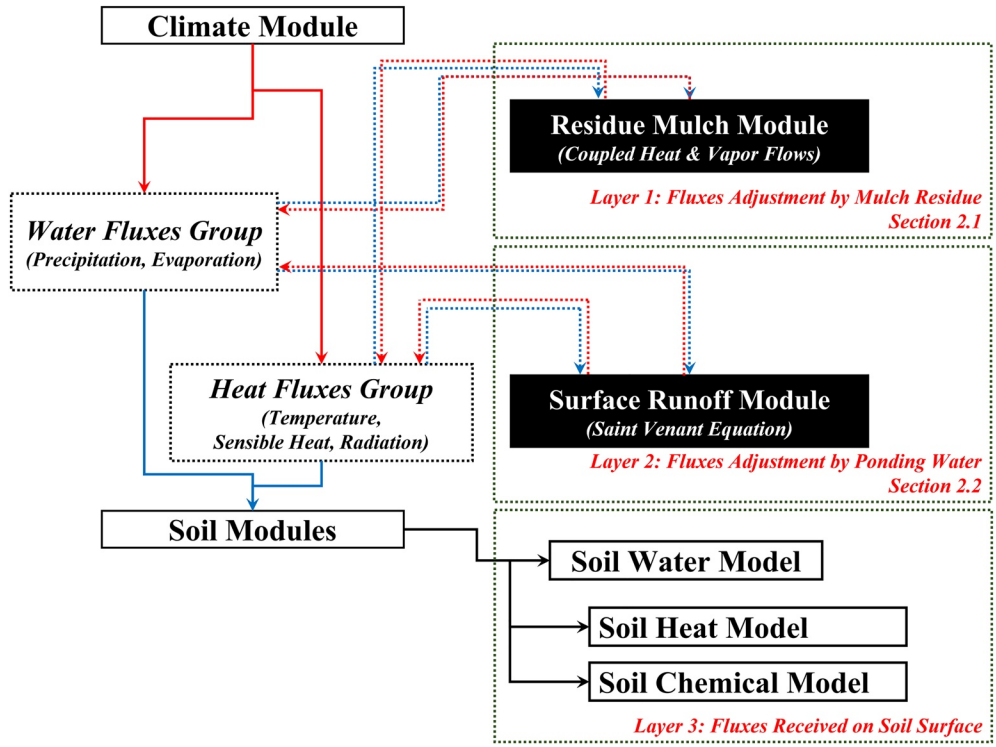

Figure 3. The implementation of the residue mulch and runoff models within MAIZSIM and the data flow chart. The white boxes are the existing modules in MAIZSIM, and the solid black arrows show their dependence. The black boxes are the new modules. The dash boxes present the variables of surface water and thermal properties, which can be modified by the new models. The solid red and blue elbow arrows indicate "model-to-variable" and "variable-to-model" data flow in the existing modules, and the dashed elbow arrows indicate the additional data flow when residue mulch and runoff models are involved.

That is because the chemical composition in the residue tends to decompose at a variety of speeds based on an "easy-to-decompose" order, that is, "CARB > CELL > LIGN" (Woodruff et al., 2018).

In this study, a revised CERES-N model is adopted for mulch residue decomposition and N mineralization (Quemada et al., 1997). The CERES-N model computes the residue decomposition and N mineralization based on the whole mulch layer, and variations of decomposition and mineralization rates along the vertical direction are approximated based on a contacting factor. However, in this study, since the residue mulch is discretized into multiple elemental layers (Figure 1), we replace the contacting factor in CERES-N model with the two-layer representation used in the $\text{PASTIS}_{\text{mulch}}$ model, where residue mulch is assumed to be a contacting portion near the mulch-soil interface $\left(\mathcal{N}_{\text{c}}\right)$ and a non-contacting portion near the mulch-air interface $\left(\mathcal{N}_{\text{nc}}\right)$. Since the contacting factor and the two-layer design are mathematically homologic, we can use the contacting factor in CERES-N model to determine the boundary between the contacting and the non-contacting portions. The contacting portion occupies 45%–100% of the whole mulch layer based on the initial mulch thickness (Carley, 2021; Thapa, unpublished data). With the division of the whole residue mulch into contacting and non-contacting portions, as well as the pre-defined thickness of each elemental layer in the residue mulch grid (Figure 1), it is straightforward to determine whether an elemental layer $\left(k\right)$ belongs, or partially belongs to the contacting portion $\left[\left(k\right) \in \mathcal{N}_{\text{c}}\right]$ or the non-contacting portion $\left[\left(k\right) \in \mathcal{N}_{\text{nc}}\right]$.

For a given element, for example, $\left(k,l\right)$ in Figure 1, the residue mass is divided into three separate pools: CARB, CELL, and LIGN. The sum of the residue mass in those three pools is equal to the total residue mass in the given element, that is,

$$\text{RM}_{\text{T},(k,l)} = \text{RM}_{\text{CARB},(k,l)} + \text{RM}_{\text{CELL},(k,l)} + \text{RM}_{\text{LIGN},(k,l)} = \rho_m V \tag{18}$$

In Equation 18, $\mathrm{RM}_{\mathrm{pool},(k,l)}\left(\mathrm{g}\right)$, pool = CARB, CELL, and LIGN represents residue mass for each pool. $\mathrm{RM}_{\mathrm{T},(k,l)}\left(\mathrm{g}\right)$ is the total residue mass in the given element. $V\left(\mathrm{m}^3\right)$ is the element volume, which can be computed based on the residue mulch grid (Figure 1, with an assumption that the 2-D grid is of 1 cm thick in the third dimension). In this study, the mass fractions of C within the three residue pools follow a universal constant, for example, ~ 0.41 g g^{-1} (Tang et al., 2018). However, due to N immobilization, humification, and the change of residue quality (e.g., C/N ratio), mass fractions of N associated with the residue pools can vary during the simulations. Hence, the N mass associated with CARB, CELL, and LIGN should be traced as three N mass pools during the simulation, respectively. Note that "N associated with the residue pools" does not indicate N is within the chemical structure of carbohydrate, cellulose, or lignin. The sum of the N mass from the three N mass pools is equal to the total N mass within the given element, that is,

$$\mathrm{RM}N_{\mathrm{T},(k,l)} = \mathrm{RM}N_{\mathrm{CARB},(k,l)} + \mathrm{RM}N_{\mathrm{CELL},(k,l)} + \mathrm{RM}N_{\mathrm{LIGN},(k,l)} \tag{19}$$

where $\mathrm{RM}N_{\mathrm{pool},(k,l)}\left(\mathrm{g}\right)$ represents residue N mass for each pool, and $\mathrm{RM}N_{\mathrm{T},(k,l)}\left(\mathrm{g}\right)$ is the total N mass in the given element.

Given a horizontal element, for example, $\left(l\right)$ in Figure 1, within the contacting portion, the residue decomposition rates $\left(R_{\mathrm{dcmp,pool}}, \mathrm{g\ d}^{-1}\right)$ and the gross N mineralization rates $\left(RN_{\mathrm{mine,g,pool}}, \mathrm{g\ d}^{-1}\right)$ for individual pools are determined by intrinsic rates and adjustments, that is,

$$\begin{cases} R_{\mathrm{dcmp,pool}} = \underbrace{\left(d_{\mathrm{pool}} \sum\limits_{(k)\in\mathcal{N}_{\mathrm{c}}} \mathrm{RM}_{\mathrm{pool},(k,l)}\right)}_{\text{intrinsic rate}} \times \underbrace{\left(\mathrm{MTRF}\cdot\mathrm{CNRF}\right)}_{\text{adjustments}} \\ RN_{\mathrm{mine,g,pool}} = \underbrace{\left(d_{\mathrm{pool}} \sum\limits_{(k)\in\mathcal{N}_{\mathrm{c}}} \mathrm{RM}N_{\mathrm{pool},(k,l)}\right)}_{\text{intrinsic rate}} \times \underbrace{\left(\mathrm{MTRF}\cdot\mathrm{CNRF}\right)}_{\text{adjustments}} \end{cases} \tag{20}$$

where $l = 1,2,\ldots,L.\left(k\right) \in \mathcal{N}_{\mathrm{c}}$ represents that the sum is calculated for all of the elements within the contacting portion. In Equation 20, $d_{\mathrm{pool}}\left(\mathrm{d}^{-1}\right)$ is the first-order decay coefficient. $d_{\mathrm{pool=LIGN}}$ is assumed to be constant; while for CARB and CELL, d_{pool} values are functions with respect to the mass fraction of LIGN, that is,

$$\begin{cases} d_{\mathrm{pool=CARB}} = D_{\mathrm{CARB}} \cdot \exp\left(-\gamma \times \dfrac{\mathrm{RM}_{\mathrm{LIGN}}}{\mathrm{RM}_{\mathrm{T}}}\right) \\ d_{\mathrm{pool=CELL}} = D_{\mathrm{CELL}} \cdot \exp\left(-\gamma \times \dfrac{\mathrm{RM}_{\mathrm{LIGN}}}{\mathrm{RM}_{\mathrm{T}}}\right) \\ d_{\mathrm{pool=LIGN}} = D_{\mathrm{LIGN}} \end{cases} \tag{21}$$

$D_{\mathrm{CARB}}\left(\mathrm{d}^{-1}\right)$, $D_{\mathrm{CELL}}\left(\mathrm{d}^{-1}\right)$, $D_{\mathrm{LIGN}}\left(\mathrm{d}^{-1}\right)$, and γ are empirical coefficients. The adjustments, that is, $\mathrm{MTRF}, \mathrm{CNRF} \in \left[0,1\right]$, present the variations of decomposition and mineralization rates with respect to mulch water potential, temperature, and C/N ratio (Thapa et al., 2021a; Woodruff et al., 2018),

$$\begin{aligned} \mathrm{MTRF} &= \begin{cases} \left(a_{\mathrm{MTRF}} + b_{\mathrm{MTRF}}T\right)\cdot\exp\left[\left(c_{\mathrm{MTRF}} + d_{\mathrm{MTRF}}T^{-1}\right)\cdot h\right], & T > 0^{\circ}\mathrm{C} \\ 0, & T \le 0^{\circ}\mathrm{C} \end{cases} \\ \mathrm{CNRF} &= \begin{cases} \exp\left(-a_{\mathrm{CNRF}} \times \dfrac{\mathrm{CNR} - \mathrm{CNR}_{\mathrm{crit}}}{\mathrm{CNR}_{\mathrm{crit}}}\right), & \mathrm{CNR} > \mathrm{CNR}_{\mathrm{crit}} \\ 1, & \mathrm{CNR} \le \mathrm{CNR}_{\mathrm{crit}} \end{cases} \end{aligned} \tag{22}$$

where a_{MTRF},b_{MTRF}, c_{MTRF}, d_{MTRF} and a_{CNRF} are empirical coefficients; $\mathrm{CNR}_{\mathrm{crit}}$ is the critical mulch C/N ratio. In order to apply Equation 22, the units of mulch temperature and water potential obtained in Equation 1 should be converted from "K" and "meter of water" to "℃" and "MPa." CNR represents the overall C/N ratio in the contacting portion rather than the C/N ratio of individual residue pools, that is, $\mathrm{CNR} = 0.41 \times \mathrm{RM}_{\mathrm{T}} / \left(\mathrm{RM}N_{\mathrm{T}} + N_{\mathrm{Inorg}}\right)$, where $N_{\mathrm{Inorg}}\left(\mathrm{g}\right)$ is the quantity of mineral (microbe-available) N in

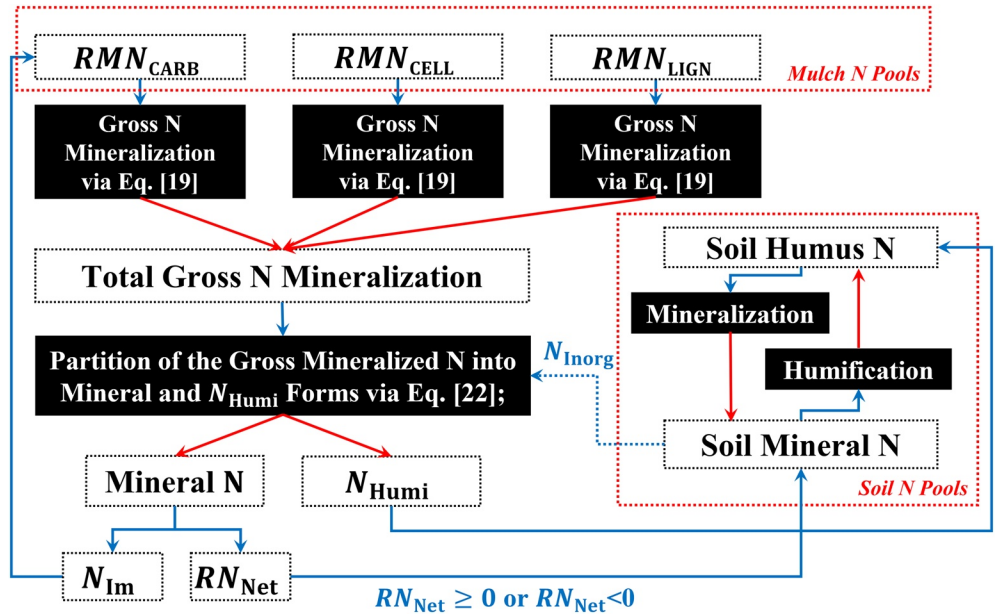

Figure 4. The N dynamics between the residue mulch and the surface soil. The white (dashed) boxes indicate the N quantities, while the black boxes indicate the processes. The solid red arrows present "process-to-quantity" paths, and the blue elbow arrows present "quantity-to-process" or "quantity-to-quantity" paths. The two dashed red boxes delineate the N pools in the residue mulch and the soil-N model imbedded in MAIZSIM, respectively. We use a dashed blue arrow to indicate that N_{Inorg} represents a "potential quantity of N exchanges", since N_{Inorg} is the input of the "min" operator in Equation 23 and may or may not be equal to the actual amount of N flow between the residue mulch and the surface soil. For example, in Equation 23, if $N_{\text{Inorg}} / \Delta t < 0.0213 \sum_{\text{pool}} R_{\text{dcmp,pool}} - \sum_{\text{pool}} RN_{\text{mine,g,pool}}$, then N_{Inorg} will affect the N exchanges between the residue mulch and the surface soil; if $N_{\text{Inorg}} / \Delta t > 0.0213 \sum_{\text{pool}} R_{\text{dcmp,pool}} - \sum_{\text{pool}} RN_{\text{mine,g,pool}}$, then the N exchanges will be governed by $0.0213 \sum_{\text{pool}} R_{\text{dcmp,pool}} - \sum_{\text{pool}} RN_{\text{mine,g,pool}}$. The actual N flow is carried by RN_{Net} and N_{Humi}. If $RN_{\text{Net}} > 0$, a net N mineralization occurs from the residue mulch to the surface soil; if $RN_{\text{Net}} < 0$, a net N mineralization occurs from the surface soil to the residue mulch.

surface soil. Therefore, based on Equation 20, the total mass change of residue mulch is $\sum_{\text{pool}} R_{\text{dcmp,pool}} \Delta t$ and the gross mass change in N is $\sum_{\text{pool}} RN_{\text{mine,g,pool}} \Delta t$.

Since N-immobilization (N_{Im}, g d^{-1}, usually happens within residue mulch) and N-humification (N_{Humi}, g d^{-1}, with a coefficient, HUMF, which converts the gross N mineralization rate to the humification rate, see Equation 23 and Figure 4) occur instantaneously during mulch decomposition, the gross N mineralization rates should be further adjusted to the net N mineralization, that is,

$$\begin{cases} N_{Im} = \max\left\{\min\left[\left(0.0213 \sum_{\text{pool}} R_{\text{dcmp,pool}} - \sum_{\text{pool}} RN_{\text{mine,g,pool}}\right), \dfrac{N_{\text{Inorg}}}{\Delta t}\right], 0\right\} \\ RN_{\text{Net}} = \left(1 - \text{HUMF}\right) \sum_{\text{pool}} RN_{\text{mine,g,pool}} - N_{Im} \\ N_{\text{Humi}} = \text{HUMF} \sum_{\text{pool}} RN_{\text{mine,g,pool}} \end{cases} \quad (23)$$

RN_{net} (g d^{-1}) indicates the net mineralized N from residue mulch to surface soil; N_{Humi} is the quantity of the instantaneous N humification during mulch decomposition, and it can be added to the humified N pools in the soil-N model. The occurrence of N_{Im} may lead to an increase of N concentration in residue mulch. When $RN_{\text{net}} > 0$, the net mineralized N migrates from residue mulch to soil; when $RN_{\text{net}} < 0$, a net N immobilization occurs from surface soil to residue mulch, such an effect may be profound for residues of relatively poor quality, that is, the residues of relatively large C/N ratio (Wells et al., 2017; Williams et al., 2018). The immobilized N returned from surface soil to residue mulch is mostly stored within the rapid decomposition pools, for example, CARB (Carley, 2021; Thapa, unpublished data). An illustrative diagram of N dynamics between soil and residue mulch is presented in Figure 4.

Within the non-contacting portion, we assume the decrease of residue mass is not due to decomposition, but to the downward transport of raw organic materials (also known as the "feeding process" defined in EXPERT-N or PASTIS$_{\text{mulch}}$ models). This transport is governed by the total decrease of residue and N mass in the contacting portion and a pre-specified feeding rate α_F. Therefore, the net changes in residue mass and N mass in the non-contacting portion can be presented as

$$\begin{cases} \sum\limits_{(k)\in\mathcal{N}_{\text{nc}}} \text{RM}_{\text{pool},(k,l)} \leftarrow \max\left[\sum\limits_{(k)\in\mathcal{N}_{\text{nc}}} \text{RM}_{\text{pool},(k,l)} - \alpha_F \Delta t \sum\limits_{\text{pool}} R_{\text{dcmp,pool}}, 0\right] \\ \sum\limits_{(k)\in\mathcal{N}_{\text{nc}}} \text{RM}N_{\text{pool},(k,l)} \leftarrow \max\left[\sum\limits_{(k)\in\mathcal{N}_{\text{nc}}} \text{RM}N_{\text{pool},(k,l)} - \alpha_F \Delta t \sum\limits_{\text{pool}} RN_{\text{mine,g,pool}}, 0\right] \end{cases} \tag{24}$$

where $\alpha_F \Delta t \sum\limits_{\text{pool}} R_{\text{dcmp,pool}}$ and $\alpha_F \Delta t \sum\limits_{\text{pool}} RN_{\text{mine,g,pool}}$, account for the mass changes as the sum for the three pools. In contrast, for the contacting portion, the mass change of each residue or N pool must be updated individually due to the variations of residue decomposition and N mineralization rates shown in Equations 20 and 23. The update rules are shown in Equation 25. All the variables in Equation 25 are defined in previous discussion, except for $F_{\text{pool, ini}}$ and $FN_{\text{pool, ini}}$. $F_{\text{pool, ini}}$ represents the initial mass fractions of a residue to the raw residue, and $FN_{\text{pool, ini}}$ represents the initial mass fractions of a N pool to total residue N.

$$\begin{cases} \sum\limits_{(k)\in\mathcal{N}_{\text{c}}} \text{RM}_{\text{pool},(k,l)} \leftarrow \max\left[\sum\limits_{(k)\in\mathcal{N}_{\text{c}}} \text{RM}_{\text{pool},(k,l)} - R_{\text{dcmp,pool}}\ \Delta t + F_{\text{pool, ini}} \alpha_F \Delta t \sum\limits_{\text{pool}} R_{\text{dcmp,pool}}, 0\right] \\ \sum\limits_{(k)\in\mathcal{N}_{\text{c}}} \text{RM}N_{\text{pool},(k,l)} \leftarrow \max\left[\sum\limits_{(k)\in\mathcal{N}_{\text{c}}} \text{RM}N_{\text{pool},(k,l)} - RN_{\text{mine,g,pool}}\ \Delta t + FN_{\text{pool, ini}} \alpha_F \Delta t \sum\limits_{\text{pool}} RN_{\text{mine,g,pool}} \right. \\ \qquad \left. + N_{\text{Im}} \Delta t \underbrace{(\text{pool} = \text{CARB})}_{\substack{\text{Boolean Value for} \\ \text{True}(1) \text{ or False}(0)}}, 0\right] \end{cases} \tag{25}$$

Finally, the updated residue and N mass in the contacting and non-contacting portions, that is, $\sum\limits_{(k)\in\mathcal{N}_{\text{c}}} \text{RM}_{\text{pool},(k,l)}$, $\sum\limits_{(k)\in\mathcal{N}_{\text{nc}}} \text{RM}_{\text{pool},(k,l)}$, $\sum\limits_{(k)\in\mathcal{N}_{\text{c}}} \text{RM}N_{\text{pool},(k,l)}$, and $\sum\limits_{(k)\in\mathcal{N}_{\text{nc}}} \text{RM}N_{\text{pool},(k,l)}$, are redistributed to all the elements, based on the volume of individual elements and the thickness of the contacting and non-contacting portions.

Mulch decomposition affects the coupled heat and water transfer model in Section 2.1, as well as the soil surface water and temperature in the following two ways. (a) The water characteristic function of residue mulch may change since the residue loses cellular structures during decomposition, and the expression of water characteristic function can be related to chemical compositions of residue mulch. (b) Mulch thickness decreases (i.e., residue mulch shrinkage) due to residue decomposition, which changes the geometrical configuration of the grid in Figure 1.

In the numerical implementation, for (a), mass fraction of LIGN is used as an apparent proxy for water properties, and water characteristic function of mulch residue is expressed in a form similar to Campbell's equation (Thapa et al., 2021b). Saturated water content can also be expressed as a function with respect to mass fraction of LIGN (Thapa et al., 2021b).

$$\begin{cases} h_{(k,l)} = a_m \cdot \left[\theta_{(k,l)} \rho_w / \rho_m\right]^{-b_m} \\ \left[\theta_{(k,l)} \rho_w / \rho_m\right]_{\text{sat}} = a_{\text{sat,1}} \cdot \exp\left[-a_{\text{sat,2}} \times \text{RM}_{\text{LIGN},(k,l)} / \text{RM}_{\text{T},(k,l)}\right] \end{cases} \tag{26}$$

where $a_m = -a_{\text{wrc,1}} \cdot \exp\left[-a_{\text{wrc,2}} \times \text{RM}_{\text{LIGN},(k,l)} / \text{RM}_{\text{T},(k,l)}\right]$, $b_m = b_{\text{wrc,1}} + b_{\text{wrc,2}} \times \text{RM}_{\text{LIGN},(k,l)} / \text{RM}_{\text{T},(k,l)}$, and $a_{\text{wrc,1}}$, $a_{\text{wrc,2}}$, $b_{\text{wrc,1}}$ and $b_{\text{wrc,2}}$ are fitting parameters determined via water characteristic function measurements; $a_{\text{sat,1}}$ and $a_{\text{sat,2}}$ are fitting parameters for the saturated gravimetric water content. In Equation 26, the unit of h is MPa; therefore, unit conversion is required before applying the water characteristic function to

Table 1
Soil Physical Properties for the Examples in Section 3

Soil layers	Layer 1	Layer 2	Layer 3
Depth range (cm)	<30	30–60	60–134
Residual water content $\left(\theta_r, \mathrm{m^3 m^{-3}}\right)$	0.052	0.044	0.045
Saturated water content $\left(\theta_s, \mathrm{m^3 m^{-3}}\right)$	0.376	0.331	0.362
van Genuchten parameter (α)	0.028	0.039	0.037
van Genuchten parameter (n)	1.390	1.402	1.530
Saturated hydraulic conductivity $\left(K_{\mathrm{sat}}, \mathrm{cm\ d^{-1}}\right)$	23.541	23.231	47.000
Soil bulk density $\left(\rho_b, \mathrm{g\ cm^{-3}}\right)$	1.570	1.720	1.610
Mass fraction of soil organic matter $\left(\mathrm{g\ g^{-1}}\right)$	0.006	0.008	0.002
Mass fraction of sand $\left(\mathrm{g\ g^{-1}}\right)$	0.660	0.740	0.760
Mass fraction of silt $\left(\mathrm{g\ g^{-1}}\right)$	0.180	0.140	0.140

Equations 1 and 2. $\left[\theta\rho_w/\rho_m\right]\left(\mathrm{g\ g^{-1}}\right)$ implies the gravimetric water content since θ is defined as the volumetric water content, and the subscript "sat" is the abbreviation of "saturation."

For (b), mulch density, ρ_m, is assumed to be constant during a simulation. Hence, for a given elemental layer, the grid shrinkage is proportional to the mass loss of residue mulch at that elemental layer. For numerical stability, a threshold is defined for the minimal thickness of each elemental layer. When the thickness of an elemental layer is smaller than that threshold, it is merged with the adjoined elemental layer (usually the upper one). When the thickness of the whole residue mulch layer is smaller than that threshold, the residue mulch can be considered as fully decomposed, such that the "Residue Mulch Module" in Figure 3, as well as the mulch decomposition model, will be deactivated automatically.

3. Illustrative Examples

In this section, illustrative examples are provided to demonstrate the model performance and how the simulated results can be interpreted. In Section 3.1, a cereal rye residue mulch is used, but residue mulch decomposition is manually switched off, such that we can evaluate the model performance on simulating the water and temperature of rigid residue mulch (i.e., non-decomposable residue mulch) and surface soil. In Section 3.2, the simulation under the same scenario as in Section 3.1 is redone, but residue decomposition, C and N exchanges between the residue mulch and the surface soil, and the mulch shrinkage with respect to time are included. Therefore, the simulation in Section 3.1 is a special case of the one in Section 3.2. However, we made Section 3.1 as a separate example in the study to enable comparisons of the model proposed in Sections 2.1–2.4 with existing studies, since most of the existing experiments and models for surface water and temperature dynamics were performed with a rigid residue mulch.

Soil and weather data were obtained from a research site in Jarrettsville, Maryland, during the 2017 growing season. Weather data included hourly radiation, temperature, wind speed, relative humidity, and precipitation. The soil in the research site was Fine-loamy, mixed, semiactive, mesic Typic Hapludults, and the physical properties are listed in Table 1. The initial residue mulch biomass was assumed to be $12\ \mathrm{t\ ha^{-1}} = 1.2\ \mathrm{kg\ m^{-2}}$, corresponding to a 6 cm uniform residue layer with bulk density and porosity equal to $20\ \mathrm{kg\ m^{-3}}$ and 0.95, respectively. Such a relatively large initial residue mulch biomass is used because (a) the residue mulch is relatively thick such that the simulated water and temperature distributions within the residue mulch can be clearly presented, and (b) some radiation and turbulence measurements are performed for relatively thick residue mulch (Novak et al., 2000, 2000a), so the measured radiation properties can be directly used in the simulations. We also assume the residue mulch was "early killed cereal rye" with

Table 2
Mulch Physical and Chemical Properties for the Examples in Section 3

Physical and chemical properties of mulch residue (synthetic data) [Refer to Carley, 2021; Findeling, Chanzy, & de Louvigny, 2003; Novak et al., 2000a; Thapa et al., 2021a, 2021b; Thapa, unpublished data]	
Mass properties	
Initial residue mulch biomass $\left(\text{g m}^{-2}\right)$	1,200
Mulch width $\left(X_m, \text{cm}\right)$	38.1
Mulch thickness $\left(Z_m, \text{cm}\right)$	6.0
Density of mulch residue $\left(\rho_m, \text{g m}^{-3}\right)$	20,000
Mulch porosity $\left(\varphi_m, \text{m}^3\ \text{m}^{-3}\right)$	0.95
Hydraulic properties	
Saturated gravimetric water content (Equation 26)	$a_m = -20.1 \cdot \exp\left[-0.249 \frac{\text{RM}_{\text{LIGN}}}{\text{RM}_{\text{T}}}\right]$ $b_m = 0.324 + 0.124 \frac{\text{RM}_{\text{LIGN}}}{\text{RM}_{\text{T}}}$
Residue water characteristic function (Equation 26)	$\left(\frac{\theta\rho_w}{\rho_m}\right)_{\text{sat}} = 7.10 \cdot \exp\left[-0.079 \frac{\text{RM}_{\text{LIGN}}}{\text{RM}_{\text{T}}}\right]$
Thermal properties	
Specific heat of mulch residue $\left(C_{m,s}, \text{J g}^{-1}\ \text{K}^{-1}\right)$	1.76
Residue thermal diffusivity $\left(D_m, \text{J m}^{-1}\ \text{K}^{-1}\ \text{s}^{-1}\right)$	0.25
Reference temperature $\left(T_{\text{ref}}, \text{K}\right)$	293.15
Radiation properties	
Residue-area index $\left(\Delta R\right)$	0.3
Clumping index $\left(\Omega_{cf}\right)$	0.6
Residue shortwave reflectivity $\left(\alpha_m\right)$	0.3
Residue longwave emissivity $\left(\varepsilon_m\right)$	1.0
Chemical and decomposition properties	
Initial mass fraction of CARB $\left(\text{g g}^{-1}\right)$	0.2
Initial mass fraction of CELL $\left(\text{g g}^{-1}\right)$	0.7
Initial mass fraction of LIGN $\left(\text{g g}^{-1}\right)$	0.1
Initial N mass fraction in CARB $\left(\text{g g}^{-1}\right)$	0.08
Initial N mass fraction in CELL $\left(\text{g g}^{-1}\right)$	0.01
Initial N mass fraction in LIGN $\left(\text{g g}^{-1}\right)$	0.01
Humification factor $\left(\text{HUMF}\right)$	0.125
Feeding rate $\left(\alpha_F\right)$	0.1
First-order decay coefficients (Equation 21)	$d_{\text{CARB}} = 0.43 \cdot \exp\left(-12.0 \frac{\text{RM}_{\text{LIGN}}}{\text{RM}_{\text{T}}}\right)$ $d_{\text{CELL}} = 0.24 \cdot \exp\left(-12.0 \frac{\text{RM}_{\text{LIGN}}}{\text{RM}_{\text{T}}}\right)$ $d_{\text{LIGN}} = 0.0228$

Table 2
Continued

Physical and chemical properties of mulch residue (synthetic data) [Refer to Carley, 2021; Findeling, Chanzy, & de Louvigny, 2003; Novak et al., 2000a; Thapa et al., 2021a, 2021b; Thapa, unpublished data]	
Water and temperature adjustment (MTRF, Equation 22)	$\mathrm{MTRF} = \begin{cases} (0.384 + 0.018T)\exp\left[\left(0.142 + \frac{0.628}{T}\right)h\right] & T > 0℃ \\ 0 & T \le 0℃ \end{cases}$
C/N ratio adjustment (CNRF, Equation 22)	$\mathrm{CNRF} = \begin{cases} \exp\left(-0.693\frac{\mathrm{CNR} - 13.0}{13.0}\right) & \mathrm{CNR} > 13.0 \\ 1 & \mathrm{CNR} \le 13.0 \end{cases}$

a relatively high N concentration (C/N ratio was 15–20), such that the performance of N mineralization can be emphasized and clearly demonstrated.

The residue mulch was initially divided into 5 elemental layers, and the thickness for each elemental layer was 1.2 cm. The physical properties of the residue mulch are summarized in Table 2. Numerical simulations were performed for a 100-day time period, that is, from April 20, 2017 (Day-of-Year, DOY = 100) to July 19, 2017 (DOY = 200). No crop was assumed to grow during the simulation period. Two relatively large rainfall events were artificially added on April 30, 2017 (DOY = 110) and June 09, 2017 (DOY = 160), with an intensity of 30 mm h^{-1} from 6:00 to 13:00. The goal of applying the artificial precipitation is to create a scenario with stable surface runoff. Hence, the model adaptability for automatic adjustments of the computing grid based on ponded water and the switch of the boundary conditions between infiltration and evaporation can be demonstrated. The maximum ponding depth held by the residue mulch was assumed to be half the mulch thickness, that is, 3.0 cm in the illustrative examples. Therefore, although the simulations are generated from real soil and weather data, the assumptions included in the simulations make the illustrative examples semi-synthetic.

The two illustrative examples were executed on a personal computer with an Intel(R) Core(TM) i9-7900X CPU (with Turbo Boost off), an HyperX(R) Predator(TM) DDR4 RAM (3600MHz) and an ASUS(R) Prime(TM) X299-Deluxe motherboard. The time consumed for the illustrative example is ~20 min in the debug mode.

3.1. Simulation of Water and Temperature of Non-Decomposable (Rigid) Residue Mulch and Surface Soil

The simulated temperature within the residue mulch during the 100-day simulation period is presented in Figure 5. In general, the temperature differences between the mulch-air interface and the mulch-soil interface are less than 3℃. The largest temperature differences mostly occurred during daytime because the mulch-air interface receives more shortwave radiation than the lower elemental layers. The amplitudes of daily temperature fluctuations decrease from the mulch-air interface to the mulch-soil interface. That is because (a) the dry residue mulch has a relatively low heat capacity, hence the upper elemental layers present instantaneous responses to ambient temperature variations; (b) compared to bare soil, the residue mulch reduces the heat flux intensity and therefore smooths the temperature variation in the lower elemental layers.

Within a multiple-day period, when the variations of daily mean temperature and the amplitudes of daily temperature fluctuations are relatively small, for example, DOY132-142 (the temperature values are demarcated by the dashed lines in Figure 5, marked and sub-plotted as [A]), the range of temperature variations for lower elemental layers tends to be within the range of temperature variations for upper elemental layers. However, when daily mean temperature follows an "increasing-then-decreasing" pattern during a multiple-day period and the daily temperature fluctuations are relatively large, for example, DOY180-194 (the temperature values are demarcated by the dashed curves in Figure 5, marked and sub-plotted as [B]), the temperature near the mulch-soil interface tends to be consistently lower than the temperature near the mulch-air interface, such that the temperature near the mulch-soil interface has the smallest variations.

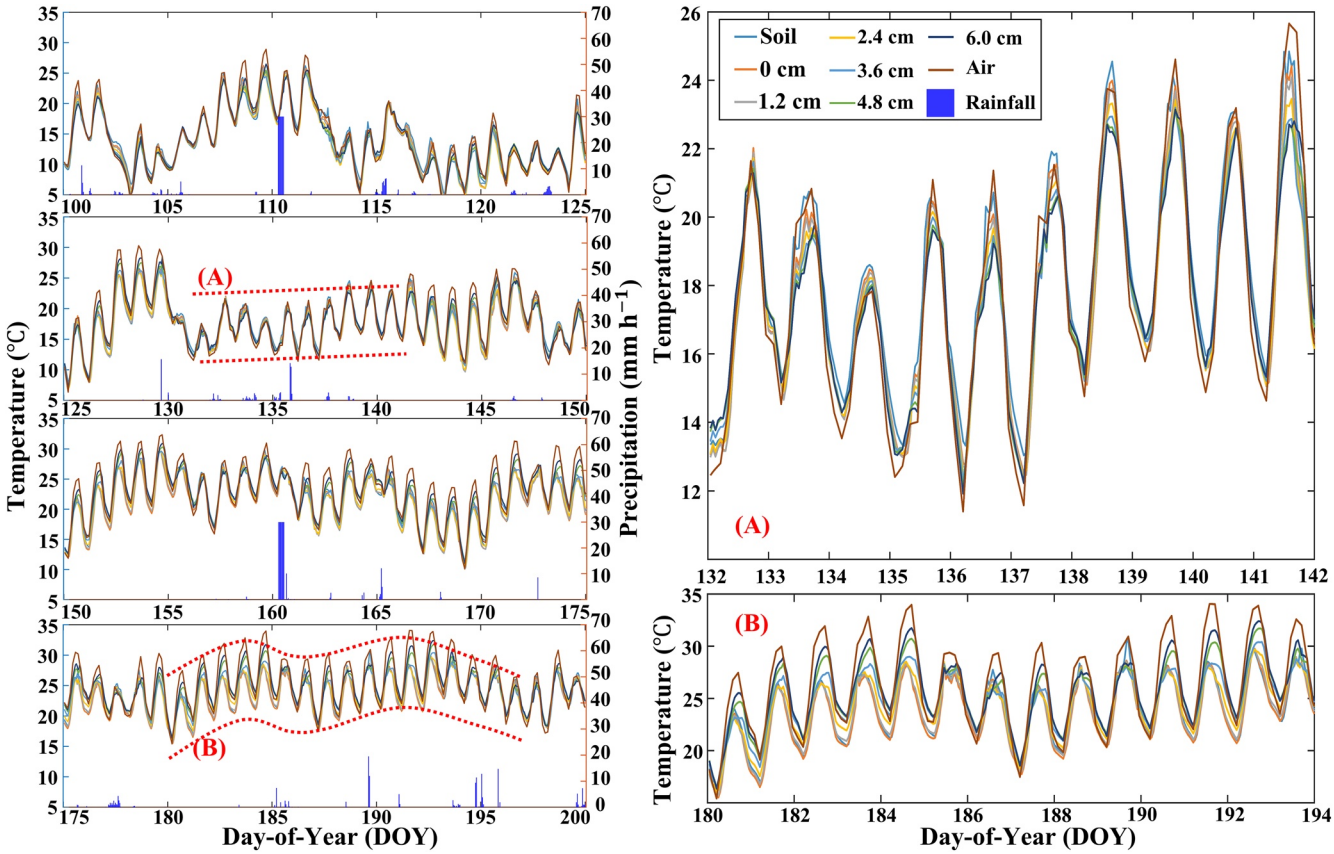

Figure 5. The simulated temperature for each mulch-layer interface during the 100-day simulation period (split into four figures, see the horizontal axis). The temperature of surface soil, the temperature of ambient air, and the precipitation are also presented. The position "0 cm" indicates the mulch-soil interface, while the position "6 cm" indicates the mulch-air interface. The dashed curves (A) and (B) demarcate two regions of interest mentioned in the paper, showing two possible multiply day temperature variation patterns, and the subplots associated with (A) and (B) are also plotted. Hereafter, precipitation is presented with a flux unit $\left(\text{mm h}^{-1}\right)$; however, it can also be understood as the cumulative precipitation $\left(\text{mm}\right)$ during a one-hour period.

Therefore, the residue mulch can not only mitigate the daily temperature fluctuations, but also regulate the temperature variations in a multiple-day scale. Yin et al. (2020) reported observed temperature patterns similar to our simulation results; but they measured the temperature not at the soil surface but as an average temperature for shallow soil layers (see Figures 1 and 2 in Yin et al., 2020).

The simulated water content within the residue mulch during the 100-day simulation period is presented in Figure 6. The volumetric water content within the residue mulch is relatively low since most of the mulch pore space is air-filled. However, instantaneous increases of the volumetric water content occur during the two artificial rainfall events. The lower elemental layers are saturated when water ponding is established, and the water content is equal to the residue porosity, that is, 0.95 $\text{cm}^3\ \text{cm}^{-3}$ (the water content values during the two artificial rainfall events are demarcated by the dashed lines in Figure 6, marked and sub-plotted as [A] and [B]). However, the water content in the upper elemental layers remains small because the maximum ponding depth is assumed to be half the mulch thickness, that is, 3 cm in this example. After precipitation is terminated, the ponded water is drained and the water content in lower elemental layers decreases to relatively small values, due to the small water holding capacity of the residue mulch.

During the two rainfall events, the water fluxes near the soil surface, as well as the ponded depth, are presented in Figure 7. The two rainfall events are identical, and the patterns of surface runoff and infiltration are similar. When the precipitation initiates, the infiltration achieves the largest value since the surface soil is not yet saturated, and the matric potential gradient governs the infiltration flux. The differences between the precipitation and infiltration fluxes contribute to water ponding on the soil surface. During the following 1.5 h, the infiltration flux decreases and approaches a stable level, and the ponded water depth increases

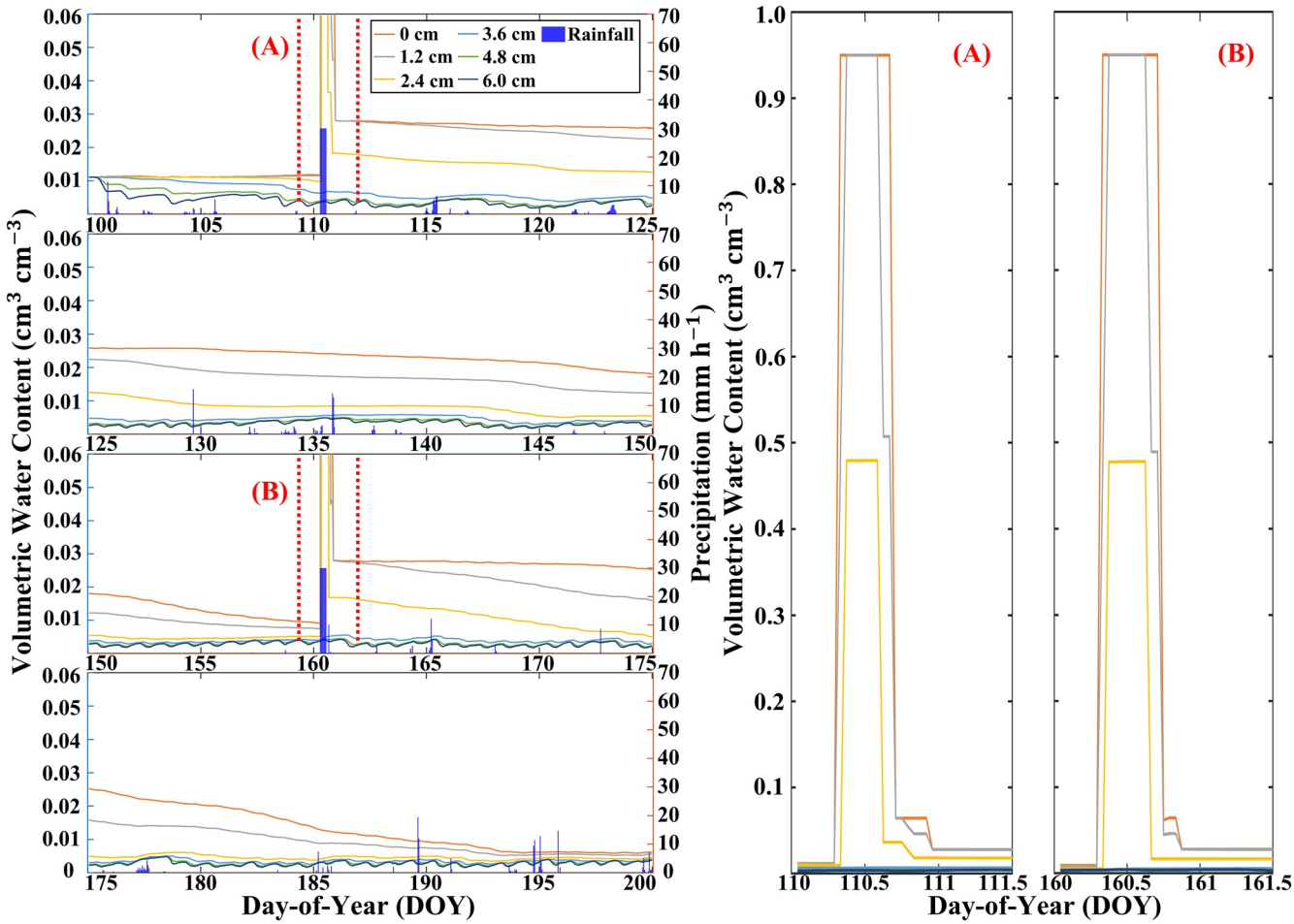

Figure 6. The simulated volumetric water content for each mulch-layer interface during the 100-day simulation period (split into four figures, see the horizontal axis). The precipitation is also presented. The position "0 cm" indicates the mulch-soil interface, while the position "6 cm" indicates the mulch-air interface. The dashed curves (A) and (B) demarcate the water content during the two artificial rainfall events, demonstrating the existence of ponded water, and the subplots associated with (A) and (B) are also plotted.

with respect to time. When the ponded water depth reaches the maximum value that can be held by the residue mulch, surface runoff occurs following Equation 16. When the rainfall event ends, the surface runoff stops but the infiltration lasts for another ~3 h, because the maximum ponding depth in this example is 3.0 cm and the stable infiltration flux is ~10 mm h^{-1} (see Figure 7 for the simulated infiltration fluxes).

Ra and Ri values are presented in Figure 8, as well as wind speed from the weather data. Most of the Ra values are 1 to 2 orders of magnitude larger than the critical value Ra = 1706, which is similar to the measurement results reported in Novak et al. (2000a) under a similar initial residue mulch biomass. Based on the Ra values obtained from the simulation, free convection for heat and vapor fluxes occurs within the mulch. Ri is highly related to the ambient wind speed. In this example, the Ri values are 1 to 2 orders of magnitude smaller than the critical value Ri = 1, indicating that the shear force provided by the wind also induces forced convection for heat and vapor fluxes.

Figure 9 shows the comparison of the simulated soil surface temperature and volumetric water content between bare soil (no residue mulch) and soil under the residue mulch. In Figure 9a, during the daytime, the residue mulch reduces the soil surface temperature by 1–5℃ compared to the air temperature, and ~10℃ compared to the bare soil surface. Two possible reasons for the relatively low surface soil temperature under the residue mulch are (a) the shortwave radiation is attenuated by the residue mulch, and (b) surface soil under the residue mulch has relatively high water content, which increases soil heat capacity and limits the increase of the surface soil temperature. During the nighttime, surface soil temperature under the residue

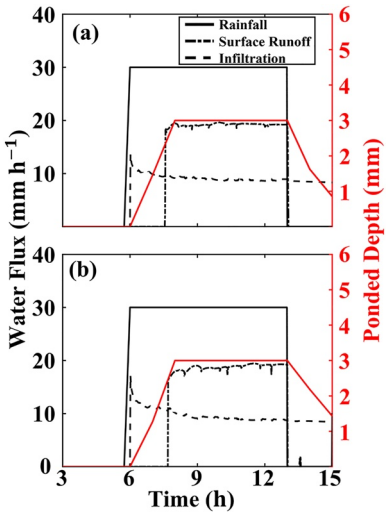

Figure 7. The precipitation flux density, surface runoff flux density and the infiltration flux density during the rainfall events on April 30, 2017 (a, DOY = 110) and the rainfall events on June 09, 2017 (b, DOY = 160). Precipitation contributes to both ponding of water and infiltration during the first 1.5 h since the rainfall starts, before runoff begins. The maximum ponding depth is 3.0 cm in this example and presented with red curves. The data are recorded 3-h before and 2-h after the two rainfall events.

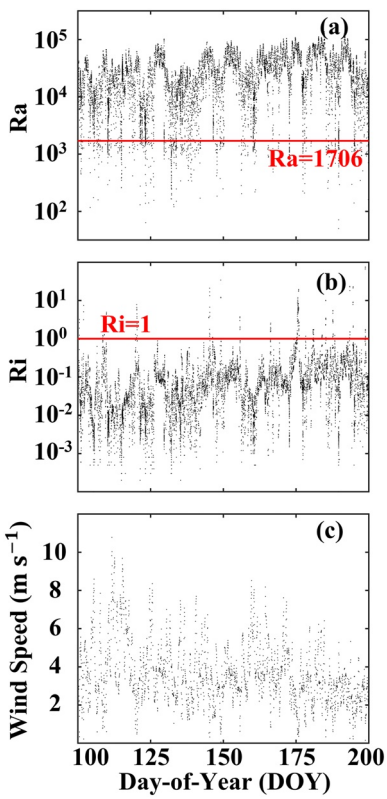

Figure 8. The calculated (a) Rayleigh number (Ra), (b) Richardson number (Ri) and (c) the wind speed above the mulch-air interface during the 100-day simulation period.

mulch is equal or slightly lower than the bare soil surface temperature, and the temperature differences among air, bare surface soil, and surface soil under the residue mulch are smaller than the temperature during the daytime. A possible reason is that without solar radiation (shortwave radiation), thermal equilibrium can be reached between the bare surface and the ambient air, or between the mulched surface and the ambient air. Slightly lower temperature for the surface soil under the residue mulch is possibly due to the relatively high water content conserved by the residue mulch, and relatively slow response to the changes in ambient temperature, especially when the temperature follows a multiple-day upward trend, for example DOY = 125–130, DOY = 150–155, and DOY = 180–187. Similar temperature variations can be found in Figure 7 in Liu et al. (2014) and Figure 2 in Yin et al. (2020); however, the time scale in their measurements is larger than the time scale presented in this example. In general, during the simulation period (late spring and early summer), the bare soil temperature is higher than that of the mulched soil regardless the fluctuations of the ambient temperature.

For soil surface water content shown in Figure 9b, during rainfall events, precipitation infiltrates into both the mulched and bare soil surfaces and generates similar water content values. Especially for the two artificial rainfall events, surface soil water contents in both cases reach their saturated values. However, after rainfall events, the water content in the bare surface soil decreases more rapidly than the water content in the soil under the residue mulch. Most of the mulch induced water conservation effects occur during the daytime. For example, during DOY = 140–147 or DOY = 178–185, without the residue mulch, water content in the surface soil drops during the daytime due to evaporation, and during the nighttime, the surface water is recharged by capillary rise from deeper soil water and lost through evaporation in the following days, until the water content for the whole soil profile decreases and achieves a stable water content distribution. With the residue mulch, the daytime evaporation is inhibited, such that relatively large amounts of water can be stored in both surface soil and deep soil profiles. A similar result can be found in Figure 5 in Liu et al. (2014), where the variations of soil water storage were measured among multiple dry and wet seasons. Liu et al. (2014) showed that during wet seasons (corresponding to the rainfall period in our simulation), the soil water content for mulched soil and bare soil were similar; while during the dry season (corresponding to the period between two rainfall events in our simulation), water stored in the bare soil was 60%–90% of the water stored in the mulched soil.

3.2. Simulation of Mulch Decomposition and Nitrogen Mineralization

In this simulation, the weather conditions and soil properties are the same as in Section 3.1, except that the mulch decomposition model in Section 2.5 is invoked. The patterns of temperature and water content variations within the mulch and surface soil, as well as the surface runoff are similar to those shown in Section 3.1, since thickness of the residue mulch is >4 cm by the end of the simulation (see Figure 10). Furthermore, the mechanisms of the residue mulch effects on surface water content and temperature are of the same as the ones in Section 3.1. Therefore, we omit the discussion on the water and thermal dynamics but focus on the changes in the residue mulch itself. The simulated mulch and soil

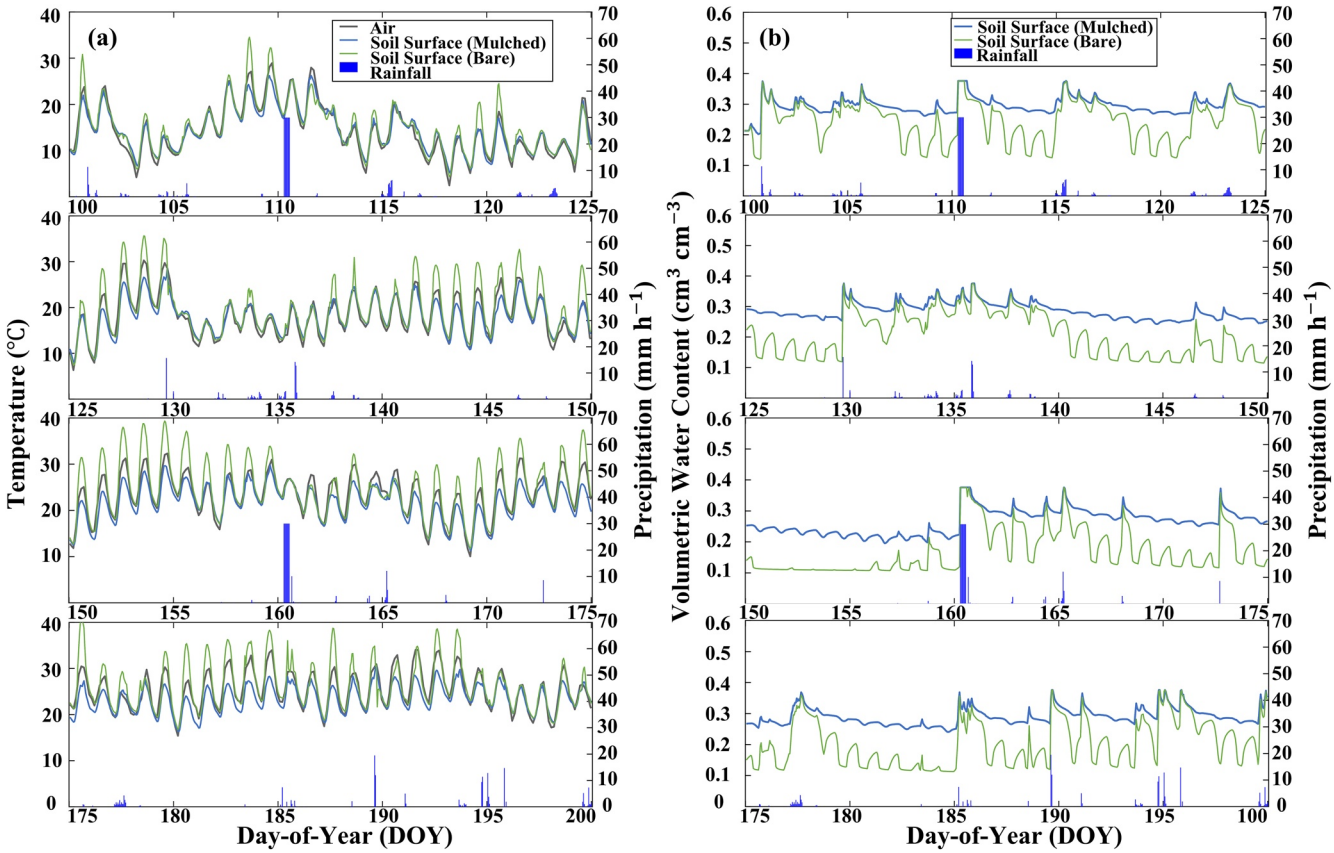

Figure 9. The simulated temperature (a, left column) and the simulated volumetric water content (b, right column) of the surface soil with or without the residue mulch during the whole 100-day period. The air temperature and the precipitation are also presented. In the figure, the surface soil is defined as the layer from the soil surface to 5.0 cm depth.

water contents and temperatures with the decomposing residue mulch can be found in the numerical example files released together with this paper (see Data Availability Statements).

The changes in thickness of each mulch elemental layer with respect to time are shown in Figure 10, The curves in Figure 10 present the vertical positions of the mulch-layer interfaces, labeled from the mulch-soil interface to the mulch-air interface (refer to Figure 1). The distance between adjacent curves represents the thickness of the corresponding mulch elemental layer. The mulch-soil interface is used as the reference vertical position, that is, $z = 0$. The thickness of the whole residue mulch layer is shown as the difference

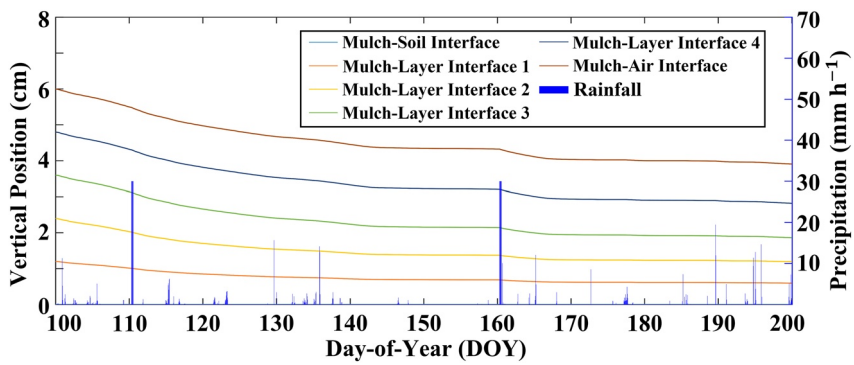

Figure 10. The vertical position of each mulch-layer interface during the 100-day simulation, including the mulch-soil interface and the mulch-air interface. The results indicate the shrinkage of each mulch elemental layer.

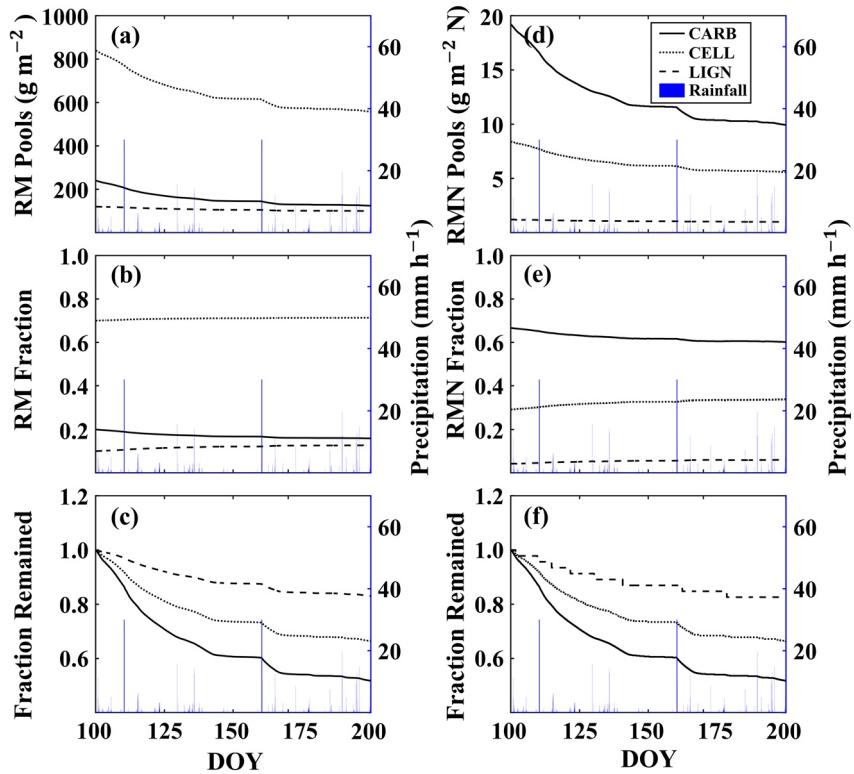

Figure 11. (a and d) The changes of residue mass pools (RM, left column) and N mass pools (RMN, right column) during the 100-day simulation; (b and e) the mass fractions of each RM and RMN pool with respect to the total residue mass and N mass of the residue mulch; (c and f) the remaining fraction of each RM and RMN pool with respect to their initial value.

between the reference vertical position and the vertical position of the mulch-air interface. The residue decomposition and N mineralization are presented in Figure 11. In order to elucidate the absolute reduction of residue mulch mass or N mass, as well as the mass fraction changes of each residue or N pool, the figures are presented in three ways. Figures 11a and 11d show the mass variations of the residue and N pools during the 100-day simulation; Figures 11b and 11e show the mass fractions of each residue pool with respect to the total residue mass and the mass fractions of each N pool with respect to the total N mass; Figures 11c and 11f present the ratios of residue and N remained relative to their initial mass for all of the residue and N pools.

In general, the decomposition rates decrease with respect to time, because the mass of rapid decomposition components, such as CARB, drop during the early stage of the simulation, while the slow decomposition components, such as LIGN, remain within the residue mulch until the middle or late stage of the simulation. Two accelerated segments occur after the two artificial rainfall events, and each of them lasts for ~3 days, which demonstrates how the increase of water content promotes the residue decomposition and N mineralization. After the 100-day simulation, the elemental layers 1 and 2, which belong to the contacting portion, are shrunk by ~50%, while the total mulch layer is shrunk by ~35%. The simulated shrinking percentages are similar to the measurement results reported in Dietrich et al. (2019), although the weather, soil, and mulch conditions between this illustrative example and Dietrich et al. (2019) are not the same.

The residue decomposition and associated N mineralization can serve as a source of soil mineral N, while the variations of mass fractions of each residue or N mass pool lead to a change of mulch quality measured by the residue C/N ratio. After the 100-day simulation, 10.76 g m^{-2} of mineral N and 1.34 g m^{-2} of humified N migrate from the residue mulch to the surface soil, and the C/N ratio of the residue mulch increases from 17.08 to 19.07. Combined with Figure 11, the increase in residue C/N ratio is due to the decompositions of the CARB pool, because the CARB pool occupies only ~20% of the total residue mass but contributes ~50%

of the total N mass, and it is rapidly decomposed during the early stage of the simulation. Therefore, the rapid decomposition of CARB, as well as the amount of N released from CARB reduces the overall N mass fraction with respect to the total residue mass. The variations of the C/N ratio, as well as the mass fraction of the CARB, CELL and LIGN pools during the residue decomposition and N mineralization, are also referred to as the residue quality (Tian et al., 2007). A high-quality residue usually has a relatively low C/N ratio, hence it becomes an efficient N supplier to the surface soil (Parton et al., 2007; Taylor et al., 1989; Truong et al., 2019). Therefore, during the residue decomposition, the quality of the mulch residue degrades. Similar residue decomposition patterns and increases of C/N ratio were reported in Figures 1 and 2 and Table 7 in Halde and Entz (2016) and Figure 5 in Dietrich et al. (2019) based on their field experiments.

4. Summary and Conclusion

Rapid water (liquid and vapor) and heat fluxes occur at soil surfaces, and these physical processes can be manipulated by field management such as residue mulch, or instantaneous events such as surface runoff. Direct measurements near the soil surface are challenging; therefore, numerical simulations are useful to investigate the water and temperature dynamics at soil surfaces. In this study, we establish a model that can perform simulations of water content and temperature at soil surfaces with residue mulch and surface runoff. The interactions between residue mulch and surface runoff, and residue decomposition as a derivative process of residue mulch are also included. The model developed in this study is deployed within a comprehensive soil-crop simulation package, MAIZSIM. Two numerical examples are presented to demonstrate the model performance with a given cereal rye residue mulch. The first example illustrates that the simulations of water and temperature in soil along with runoff within the rigid residue mulch (non-decomposable residue mulch). The second example presents the residue decomposition and N mineralization patterns during the water and temperature simulations. Plausible results are provided in the two examples, which showed (a) the residue mulch effects on conserving water and mitigating temperature variations in the surface soil, (b) the occurrence of surface runoff during relatively large rainfall events and the corresponding increases in soil surface water content, and (c) the decreasing of mulch residue decomposition rate and the changes of residue quality with respect to time. Therefore, the workability of the models designed in this study is illustrated.

The major accomplishment of this study is the establishment of the model, while in future studies, the model should be calibrated based on measurement results, for example, precipitation interception, heat and vapor transfer, and radiation attenuation, such that it can make predictions for the mulch effects under a variety of field conditions. Another accomplishment is the "layered module architecture" for model implementation, which enables (a) adaptive activations or deactivations of individual factors, for example, residue mulch and surface runoff, based on soil and weather conditions, and (b) simple extensions for additional surface and subsurface processes, for example, tillage, surface irrigation, surface fertilization or soil C models. Thus, future research topics should also include (a) embedding more physical and biochemical processes, especially agricultural field management practices, tillage that can mix surface soil and residue materials, and field C budget, within this given "layered module architecture" to support a comprehensive understanding of the physical, chemical, and biological processes that occur in surface soils, and (b) optimizing the computing efficiency of the "layered module architecture," such as the choice of the local time step, to accelerate the model and enhance its ability for large spatial scale simulations.

Conflict of Interest

The authors declare no conflicts of interest relevant to this study.

Data Availability Statement

The numerical implementation of the model established in the paper is released with the latest version of MAIZSIM at (https://github.com/ARS-CSGCL-DT), which will be updated recursively; while a concise executable version of the model, as well as the illustrative examples files, is available at (https://github.com/cauwzj). The dataset and model proposed in this study will also be available at a zenodo repository, associated with this paper published through Water Resource Research.

Acknowledgments
This study is based upon work supported by the Department of Agriculture, Agricultural Research Service under Agreement No. 58-8042-7-067; USDA National Institute of Food and Agriculture under Award No. 2018-68011-28372; USDA National Institute of Food and Agriculture under Award No. 2019-68012-29818; National Science Foundation under Grant 2037504; USDA-NIFA Multi-State Project 4188. The authors also received support from the University of Maryland, College Park, University of Nebraska, Lincoln, and Iowa State University.

References

Allen, R. G., Pereira, L. S., Raes, D., & Smith, M. (1998). *Crop evapotranspiration—Guidelines for computing crop water requirements*. FAO irrigation and drainage paper 56. Food and Agriculture Organization of the United Nations. Retrieved 2007-10-08.

Appels, W. A., Bogaart, P. W., & van der Zee, S. E. A. T. M. (2011). Influence of spatial variations of microtopography and infiltration on surface runoff and field scale hydrological connectivity. *Advances in Water Resources*, *34*, 303–313. https://doi.org/10.1016/j.advwatres.2010.12.003

Azooz, R. H., Lowery, B., Daniel, T. C., & Arshad, M. A. (1997). Impact of tillage and residue management on soil heat flux. *Agricultural and Forest Meteorology*, *84*, 207–222. https://doi.org/10.1016/S0168-1923(96)02364-7

Berkenkamp, A., Priesack, E., & Munch, J. C. (2002). Modelling the mineralisation of plant residues on the soil surface. *Agronomie*, *22*, 711–722. https://doi.org/10.1051/agro:2002042

Bristow, K. L., Campbell, G. S., Papendick, R. I., & Elliott, L. F. (1986). Simulation of heat and moisture transfer through a surface residue-soil system. *Agricultural and Forest Meteorology*, *36*, 193–214. https://doi.org/10.1016/0168-1923(86)90035-3

Cabrera, M. L., Kissel, D. E., & Vigil, M. F. (2005). Nitrogen mineralization from organic residues: Research opportunities. *Journal of Environmental Quality*, *34*, 75–79. https://doi.org/10.2134/jeq2005.0075

Campbell, G. S., & Norman, J. M. (1998). *An introduction to environmental biophysics* (2nd Ed.). Springer-Verlag New York, Inc.

Carley, M. (2021). *Modeling water relations and N mineralization from surface cover crops residues* [Master Thesis, University of Georgia].

Chavent, G., & Roberts, J. E. (1991). A unified physical presentation of mixed, mixed-hybrid finite elements and standard finite difference approximations for the determination of velocities in waterflow problems. *Advances in Water Resources*, *14*, 329–348. https://doi.org/10.1016/0309-1708(91)90020-O

Chen, W., Novak, M. D., Black, A., & Lee, X. (1997a). Coherent eddies and temperature structure functions for three contrasting surfaces. Part I: Ramp model with finite microfront time. *Boundary-Layer Meteorology*, *84*, 99–124. https://doi.org/10.1023/A:1000338817250

Chen, W., Novak, M. D., Black, A., & Lee, X. (1997b). Coherent eddies and temperature structure functions for three contrasting surfaces. Part II: Renewal model for sensible heat flux. *Boundary-Layer Meteorology*, *84*, 124–147. https://doi.org/10.1023/A:1000342918158

Chung, S., & Horton, R. (1987). Soil heat and water flow with a partial surface mulch. *Water Resources Research*, *23*, 2175–2186. https://doi.org/10.1029/WR023i012p02175

Dietrich, G., Recous, S., Pinheiro, P. L., Weiler, D. A., Schu, A. L., Rambo, M. R. L., & Giacomini, S. J. (2019). Gradient of decomposition in sugarcane mulches of various thicknesses. *Soil and Tillage Research*, *192*, 66–75. https://doi.org/10.1016/j.still.2019.04.022

Enrique, G., Braud, I., Jean-Louis, T., Michel, V., Pierre, B., & Jean-Christophe, C. (1999). Modelling heat and water exchanges of fallow land covered with plant-residue mulch. *Agricultural and Forest Meteorology*, *97*, 151–169. https://doi.org/10.1016/S0168-1923(99)00081-7

Findeling, A., Chanzy, A., & de Louvigny, N. (2003). Modeling water and heat flows through a mulch allowing for radiative and long-distance convective exchanges in the mulch. *Water Resources Research*, *39*, 1124. https://doi.org/10.1029/2002WR001820

Findeling, A., Garnier, P., Coppens, F., Lafolie, F., & Recous, S. (2007). Modelling water, carbon and nitrogen dynamics in soil covered with decomposing mulch. *European Journal of Soil Science*, *58*, 196–206. https://doi.org/10.1111/j.1365-2389.2006.00826.x

Findeling, A., Ruy, S., & Scopel, E. (2003). Modeling the effects of a partial residue mulch on runoff using a physically based approach. *Journal of Hydrology*, *275*, 49–66. https://doi.org/10.1016/S0022-1694(03)00021-0

Fleisher, D. H., Haynes, K. G., & Timlin, D. J. (2020). Cultivar coefficient stability and effects on yield projections in the SPUDSIM model. *Agronomy Journal*, *112*, 828–843. https://doi.org/10.1002/agj2.20070

Gilley, J. E., Kottwitz, E. R., & Wieman, G. A. (1991). Roughness coefficients for selected residue materials. *Journal of Irrigation and Drainage Engineering*, *117*, 503–514. https://doi.org/10.1061/(ASCE)0733-9437

Halde, C., & Entz, M. H. (2016). Plant species and mulch application rate affected decomposition of cover crop mulches used in organic rotational no-till systems. *Canadian Journal of Plant Science*, *96*, 59–71. https://doi.org/10.1139/cjps-2015-0095

Ham, J. M., & Kluitenberg, G. J. (1994). Modeling the effect of mulch optical properties and mulch-soil contact resistance on soil heating under plastic mulch culture. *Agricultural and Forest Meteorology*, *71*, 403–424. https://doi.org/10.1016/0168-1923(94)90022-1

Horton, R., & Wierenga, P. J. (1983). Estimating the soil heat flux from observations of soil temperature near the surface. *Soil Science Society of America Journal*, *47*, 14–20. https://doi.org/10.2136/sssaj1983.03615995004700010003x

Kader, M. A., Senge, M., Mojid, M. A., & Nakamura, K. (2017). Mulching type-induced soil moisture and temperature regimes and water use efficiency of soybean under rain-fed condition in central Japan. *International Soil and Water Conservation Research*, *5*, 302–308. https://doi.org/10.1016/j.iswcr.2017.08.001

Kim, S., Yang, Y., Timlin, D. J., Fleisher, D. H., Dathe, A., Reddy, V. R., & Staver, K. (2012). Modeling temperature responses of leaf growth, development, and biomass in maize with MAIZSIM. *Agronomy Journal*, *104*, 1523–1537. https://doi.org/10.2134/agronj2011.0321

Kimball, B. A., Jackson, R. D., Reginato, R. J., Nakayama, F. S., & Idso, S. B. (1976). Comparison of field-measured and calculated soil-heat fluxes. *Soil Science Society of America Journal*, *40*, 18–25. https://doi.org/10.2136/sssaj1976.03615995004000010010x

Kollet, S. J., & Maxwell, R. M. (2006). Integrated surface–groundwater flow modeling: A free-surface overland flow boundary condition in a parallel groundwater flow model. *Advances in Water Resources*, *29*, 945–958. https://doi.org/10.1016/j.advwatres.2005.08.006

Kouznetsov, M. Y. (1989). *Development and use of mathematical models of water transfer at irrigated lands*. Ph.D. Thesis. Research Institute of Heat and Mass Transfer, 170pp.

Lai, S. H., Tiedje, J. M., & Erickson, A. E. (1976). In situ measurement of gas diffusion coefficient in soils. *Soil Science Society of America Journal*, *40*, 3–6. https://doi.org/10.2136/sssaj1976.03615995004000010006x

Li, S., Wang, Z., Malhi, S. S., Li, S., Gao, Y., & Tian, X. (2009). Nutrient and water management effects on crop production, and nutrient and water use efficiency in dryland areas of China. In D. L. Sparks (Ed.), *Advances in agronomy* (Vol. *102*, pp. 223–265). https://doi.org/10.1016/S0065-2113(09)01007-4

Liu, Y., Wang, J., Liu, D., Li, Z., Zhang, G., Tao, Y., et al. (2014). Straw mulching reduces the harmful effects of extreme hydrological and temperature conditions in citrus orchards. *PLoS One*, *9*, e87094. https://doi.org/10.1371/journal.pone.0087094

Novak, M. D., & Black, T. A. (1985). Theoretical determination of the surface energy balance and thermal regimes of bare soils. *Boundary-Layer Meteorology*, *33*, 313–333. https://doi.org/10.1007/BF00116682

Novak, M. D., Chen, W., & Hares, M. C. (2000). Simulating the radiation distribution within a barley-straw mulch. *Agricultural and Forest Meteorology*, *102*, 153–186. https://doi.org/10.1016/S0168-1923(00)00096-4

Novak, M. D., Chen, W., Orchansky, A. L., & Ketler, R. (2000a). Turbulent exchange processes within and above a straw mulch. Part I: Mean wind speed and turbulent statistics. *Agricultural and Forest Meteorology*, *102*, 139–154. https://doi.org/10.1016/S0168-1923(00)00095-2

Novak, M. D., Chen, W., Orchansky, A. L., & Ketler, R. (2000b). Turbulent exchange processes within and above a straw mulch. Part II: Thermal and moisture regimes. *Agricultural and Forest Meteorology*, *102*, 155–171. https://doi.org/10.1016/S0168-1923(00)00097-6

Parton, W., Silver, W. L., Burke, I. C., Grassens, L., Harmon, M. E., Currie, W. S., et al. (2007). Global-scale similarities in nitrogen release patterns during long-term decomposition. *Scientific Reports*, *315*, 361–364. https://doi.org/10.1126/science.1134853

Philip, R., & de Vries, D. A. (1957). Moisture movement in porous materials under temperature gradients. *Transactions - American Geophysical Union*, *38*, 222–232. https://doi.org/10.1029/TR038i002p00222

Poffenbarger, H. J., Mirsky, S. B., Weil, R. R., Kramer, M., Spargo, J. T., & Cavigelli, M. A. (2015). Legume proportion, poultry litter, and tillage effects on cover crop decomposition. *Agronomy Journal*, *107*, 2083–2096. https://doi.org/10.2134/agronj15.0065

Quemada, M., Cabrera, M. L., & McCracken, D. V. (1997). Nitrogen release from surface-applied cover crop residues: Evaluating the CERES-N submodel. *Agronomy Journal*, *89*, 723–729. https://doi.org/10.2134/agronj1997.00021962008900050003x

Ross, J. (1976). Radiative transfer in plant communities. In J. L. Monteith (Ed.), *Vegetation and the atmosphere, vol. 1: Principles* (pp. 13–55). Academic Press.

Ruy, S., indeling, A., & Chadoeuf, J. (2006). Effect of mulching techniques on plot scale runoff: FDTF modeling and sensitivity analysis. *Journal of Hydrology*, *326*, 277–294. https://doi.org/10.1016/j.jhydrol.2005.11.003

Savabi, M. R., & Stott, D. E. (1994). Plant residue impact on rainfall interception. *Transactions of the ASAE*, *37*, 1093–1098. https://doi.org/10.13031/2013.28180

Singh, V., & Bhallamudi, S. M. (1998). Conjunctive surface-subsurface modeling of overland flow. *Advances in Water Resources*, *21*, 567–579. https://doi.org/10.1016/S0309-1708(97)00020-1

Sui, H. J., Zeng, D. C., & Chen, F. Z. (1992). A numerical model for simulating the temperature and moisture regimes of soil under various mulches. *Agricultural and Forest Meteorology*, *61*, 281–299. https://doi.org/10.1016/0168-1923(92)90054-8

Sun, W., Fleisher, D., Timlin, D., Li, S., Wang, Z., & Reddy, V. R. (2021). Effects of elevated CO_2 and temperature on soybean growth and gas exchange rates: A modified GLYCIM model. *Agricultural and Forest Meteorology*. (Under Review).

Tang, Z., Xu, W., Zhou, G., Bai, Y., Li, J., Tang, X., et al. (2018). Patterns of plant carbon, nitrogen, and phosphorus concentration in relation to productivity in China's terrestrial ecosystems. *Proceedings of the National Academy of Sciences of the United States of America*, *115*, 4033–4038. https://doi.org/10.1073/pnas.1700295114

Taylor, B. R., Parkinson, D., & Parsons, W. F. J. (1989). Nitrogen and lignin content as predictors of litter decay rates: A microcosm test. *Ecology*, *70*, 97–104. https://doi.org/10.2307/1938416

Thapa, L., Tully, K., Cabrera, M., Dann, C., Schomberg, H. H., Timlin, D., et al. (2021b). Cover crop residue moisture content controls diurnal variations in surface residue decomposition. *Agricultural and Forest Meteorology*, *308–309*, 108537. https://doi.org/10.1016/j.agrformet.2021.108537

Thapa, R., Tully, K., Cabrera, M. L., Dann, C., Schomberg, H. H., Timlin, D., et al. (2021a). Effects of moisture and temperature on C and N mineralization from surface-applied cover crop residues. *Biology and Fertility of Soils*, *57*, 485–498. https://doi.org/10.1007/s00374-021-01543-7

Thorburn, P. J., Probert, M. E., & Robertson, F. A. (2001). Modelling decomposition of sugar cane surface residues with APSIM–Residue. *Field Crops Research*, *70*, 223–232. https://doi.org/10.1016/S0378-4290(01)00141-1

Tian, G., Badejo, M. A., Okoh, A. I., Kolawole, G. O., Hayashi, Y., & Salako, F. K. (2007). Effects of residue quality and climate on plant residue decomposition and nutrient release along the transect from humid forest to Sahel of West Africa. *Biogeochemistry*, *86*, 217–229. https://doi.org/10.1007/s10533-007-9158-3

Timlin, D. J., Pachepsky, Y. A., & Acock, B. (1996). A design for a modular, generic soil simulator to interface with plant models. *Agronomy Journal*, *88*, 162–169. https://doi.org/10.2134/agronj1996.00021962008800020008x

Truong, T. H. H., Kristiansen, P., & Marschner, P. (2019). Influence of mulch C/N ratio and decomposition stage on plant N uptake and N availability in soil with or without wheat straw. *Journal of Plant Nutrition and Soil Science*, *182*, 879–887. https://doi.org/10.1002/jpln.201900067

Unger, P. W. (Ed.), (1994). *Managing agricultural residues*. Lewis Publishers.

van Atta, C. W. (1977). Effect of coherent structures on structure functions of temperature in the atmospheric boundary layer. *Archives of Mechanics*, *29*, 161–171.

Vieira, D. C. S., Serpa, D., Nunes, J. P. C., Prats, S. A., Neves, R., & Keizer, J. J. (2018). Predicting the effectiveness of different mulching techniques in reducing post-fire runoff and erosion at plot scale with the RUSLE, MMF and PESERA models. *Environmental Research*, *165*, 365–378. https://doi.org/10.1016/j.envres.2018.04.029

Vigil, M. F., & Kissel, D. E. (1991). Equations for estimating the amount of nitrogen mineralized from crop residues. *Soil Science Society of America Journal*, *55*, 757–761. https://doi.org/10.2136/sssaj1991.03615995005500030020x

Wagger, M. G., Cabrera, M. L., & Ranells, N. N. (1998). Nitrogen and carbon cycling in relation to cover crop residue quality. *Journal of Soil and Water Conservation*, *53*, 214–218.

Wang, Z., Ankeny, M., & Horton, R. (2017). The impact of water vapor diodes on soil water redistribution. *Journal of Hydrology*, *552*, 600–608. https://doi.org/10.1016/j.jhydrol.2017.07.009

Wang, Z., Timlin, D., Kouznetsov, M., Fleisher, D., Li, S., Tully, K., & Reddy, V. R. (2020). Coupled model of surface runoff and surface-subsurface water movement. *Advances in Water Resources*, *137*, 103499. https://doi.org/10.1016/j.advwatres.2019.103499

Wang, Z., Timlin, D., Li, S., Fleisher, D., Dathe, A., Luo, C., et al. (2021). Numerical simulations of maize root growth in MAIZSIM based on a diffusive model. *Agricultural Water Management*, *254*, 106966. https://doi.org/10.1016/j.agwat.2021.106966

Wells, M. S., Reberg-Horton, S. C., Mirsky, S. B., Maul, J. E., & Hu, S. (2017). In situ validation of fungal N translocation to cereal rye mulches under no-till soybean production. *Plant and Soil*, *410*, 153–165. https://doi.org/10.1007/s11104-016-2989-8

Williams, A., Wells, M. S., Dickey, D. A., Hu, S., Maul, J., Raskin, D. T., et al. (2018). Establishing the relationship of soil nitrogen immobilization to cereal rye residues in a mulched system. *Plant and Soil*, *426*, 95–107. https://doi.org/10.1007/s11104-018-3566-0

Woodruff, L. K., Kissel, D. E., Cabrera, M. L., Hitchcock, R., Gaskin, J., Vigil, M., et al. (2018). A web-based model of N mineralization from cover crop residue decomposition. *Soil Science Society of America Journal*, *82*, 983–993. https://doi.org/10.2136/sssaj2017.05.0144

Yin, W., Chai, Q., Guo, Y., Fan, Z., Hu, F., Fan, H., et al. (2020). Straw and plastic management regulate air-soil temperature amplitude and wetting-drying alternation in soil to promote intercrop productivity in arid regions. *Field Crops Research*, *249*, 107758. https://doi.org/10.1016/j.fcr.2020.107758